J. Condensed Matter Nucl. Sci. 39 (2025) 36–83

Research Article

A Lattice-Assisted Conventional Explanation for LENR, Part I

N. L. Bowen

Colorado Mountain College, Glenwood Springs, CO, 81621, USA

Abstract

This paper presents a lattice-assisted conventional explanation for Low Energy Nuclear Reactions and Low Energy Nuclear Reactors (LENR). Using such explanations, calculations, and equations, along with the beneficial behavior and lattice assistance of the palladium-deuteride host material, the so-called "miracles" of LENR are explained. Standard physics and mathematics can explain how a Low Energy Nuclear Reactor works. This paper shows that an LENR reactor is able to create and maintain a chain reaction, similar to a conventional fission reactor. The LENR reactor is able to maintain its reactions, as long as the ^{2}D fuel levels are kept at the required high densities, and as long as the behavior of the host lattice assists in the reaction. This lattice assistance is a process by which the lattice reduces the detrimental effects of the electronic stopping action, which is an action that interferes with the transport of the energetic ions through the reactor and is an adverse effect prevalent in hot fusion reactors. The mechanism by which the LENR reactor is able to maintain its reaction is that the Coulomb barrier is overcome by the transference of kinetic energy—from the energetic child products of the previous reactions, to the cold ^{2}D. This is done via collisions of the cold ^{2}D with energetic child products. When this kinetic energy is transferred to the cold ^{2}D–occurring frequently enough and with a high enough transference of energy–then these newly energized ^{2}D ions are able to overcome the Coulomb barrier, with no unconventional physics needed to explain a subsequent ^{2}D-to-^{2}D reaction. The purpose of this paper is to confirm, with a mathematical and rigorous approach, that an LENR reactor can work and does work, using the standard explanations, calculations, and equations for nuclear reactors.

Keywords: LENR, particle scattering, nuclear reaction rates, chain reaction, lattice assistance, electron scattering.

1. Introduction and Overview of an Example Calculation of an LENR

The outline of this paper is as follows:

Section 1: Introduction and Overview of an Example Calculation for an LENR
Section 2: Scattering of child products from the two primary reactions
Section 3: Reaction rate of primary child products
Section 4: Scattering of child products from the two secondary reactions
Section 5: Subsequent ^{2}D to ^{2}D reaction and determination of chain reaction
Section 6: Conclusions

© 2025 ICCF. All rights reserved. ISSN 2227-3123

There are numerous reactions that occur within the reactor core, categorized as primary reactions, secondary reactions, and tertiary reactions. The two primary reactions are $^2D+^2D\rightarrow^3T+p$ and $^2D+^2D\rightarrow^3He+n$. The two secondary reactions are $^2D+^3T\rightarrow^4He+n$ and $^2D+^3He\rightarrow^4He+p$. The tertiary reactions occur outside of the reactor core, but still in the reactor apparatus. A fourth set of reactions may occur, both within the reactor core and the reactor body, but these reactions occur in such small numbers as to be negligible. These negligible reactions will not be discussed in this paper.

There are no gamma radiations from the primary and secondary reactions. There is no neutron suppression. There is no enhancement of the improbable $^2D+^2D\rightarrow^4He+\gamma$ reaction. There are no unusual behaviors or novel physics required to overcome Coulomb barrier. Briefly described, the mechanism is that the four child products, of the prior ^2D to ^2D reactions, collide with the cold ^2D fuel, which is inside the metal palladium (Pd) core. These collisions between the energetic ^2D and the cold ^2D must happen frequently enough and energetically enough to cause a subsequent ^2D to ^2D reaction to occur, thereby sustaining the ^2D-to-^2D reaction. For this reason, the conditions inside of the Pd core must be sufficient in terms of the ^2D density and the lattice assisted mitigation of electric stopping.

The concept of Low Energy Nuclear Reactions was first researched in the late 1980's [1]. Since then, the phenomenon has been duplicated hundreds of times by numerous researchers, in numerous laboratories throughout the world. These duplications have a wide range of variations in the apparatus and a wide range of results [2]. The phenomenon has been slow to be accepted by conventional scientists, due to a lack of a conventional explanation and a clear understanding how it works. Numerous theories have been proposed, including: theories involving quantum physics [3], [4], theories involving correlated coherence [5], [6], theories involving the Bose-Einstein condensate [7], theories involving electron screening [8], [9], and theories involving highly unusual nuclear behavior. A good overview of LENR theories can be found here [10], [11], [12]. However, there has not been a conventional theory able to explain the phenomenon.

One common type of LENR reactor is made with a palladium core, and a lithium electrolyte solution around it, wherein the lithium electrolyte has an electric current going through it to drive the ^2D ions into the palladium lattice. The apparatus is that of an electrolysis system, with a cathode of palladium and an anode of platinum submerged in an electrolytic solution of lithium salt and heavy water. Ionized deuterium is absorbed into the palladium cathode, in a process called loading, such that the deuterium is situated interstitially within the palladium lattice.

In order to continue with an example calculation, some very reasonable and realistic parameters will be chosen for a typical LENR reactor, and example calculations will be made accordingly. For this example calculation, the LENR reactor is in steady state, with one watt of power being released in the sum total of the two primary nuclear reactions. The lattice is almost fully loaded, with a 0.95-to-1 density of ^2D-to-Pd.

When a deuterium and a deuterium react in a nuclear reaction, the two primary reactions are $^2D+^2D\rightarrow^3T+p$ and $^2D+^2D\rightarrow^3He+n$, with a branching ration of 50%. The charged by-products of the two primary reactions—^3T, ^3He, and protons—do not immediately escape from the Pd lattice, but rather these ions get trapped within the lattice. The two secondary reactions are $^2D+^3T\rightarrow^4He+n$ and $^2d+^3He\rightarrow^4He+p$. A similar behavior is assumed for the charged by-products of the two secondary reactions, which are energetic ^4He ions and energetic protons. However, the excited neutrons, from both the primary and secondary reactions, are able to escape the Pd core, going into the electrolyte and through the entire apparatus. Depending on the geometry of the reactor apparatus, these excited neutrons may or may not pass through the borosilicate glass beaker and the thermal water bath surrounding the apparatus. Thus, the geometry and the materials of the reactor's supporting apparatus itself may strongly alter the number of neutrons seen by the experimentalist. This neutron behavior, and the resulting interactions, is fully explored in the companion paper, "A Lattice-Assisted Conventional Explanation for LENR, Part II".

There are numerous nuclear reactions that may occur with a reasonably large reaction rate inside the core or the entire apparatus. (Other reactions may occur, but with such small reaction rates as to be negligible.) The reactions with a relatively high reaction rate are:

^{2}D+^{2}D —> ^{3}T+p (primary1 reaction)
^{2}D+^{2}D —> ^{3}He+n (primary2 reaction)
^{2}D+^{3}T —> ^{4}He+n (secondary1 reaction)
^{2}D+^{3}He —> ^{4}He+p (secondary2 reaction)
^{1}H+n —> ^{2}D+γ (tertiary reaction)
^{3}He+n—>^{3}T+p (tertiary reaction)
^{6}Li+n—>^{4}He+^{3}T (tertiary reaction)
^{7}Li+n—>^{4}He+^{3}T+n (tertiary reaction)

The tertiary reactions listed above will be considered in detail in a companion paper, "A Lattice-Assisted Conventional Explanation for LENR, Part II".

Another important type of interaction between nuclei is scattering interactions. Energetic ions scatter off the non-energetic ^{2}D inside the core. This scattering causes a slowdown of the energetic projectile ions, simultaneously transferring high kinetic energy to the target ^{2}D particle. In other words, when a high energy particle collides with another low energy particle, a transfer of kinetic energy occurs from the high energy particle to the low energy particle, thereby exciting the low energy particle to a higher kinetic energy state.

When a ^{2}D+^{2}D nuclear reaction occurs inside the Pd core, the released energy is in the form of kinetic energy of the newly-formed nuclear particles. With each collision between an energetic ion and the Pd atoms of the lattice, negligible energy will be transferred to the lattice; this is because of the larger mass difference between the light-weight energetic particles and the heavier palladium atoms bound together within the lattice. Thus, most of the released kinetic energy will stay inside the core, in the form of additional kinetic energy of the ^{2}D atoms. If the conditions inside the core are right, the reaction can then maintain its own reaction with minimal input energy. This is called a self-sustained reaction, also known as a chain reaction. When a ^{2}D+^{2}D nuclear reaction occurs inside the Pd core, the released energy is in the form of kinetic energy of the newly-formed nuclear particles. With each collision between an energetic ion and the Pd atoms of the lattice, negligible energy will be transferred to the lattice; this is because of the larger mass difference between the light-weight energetic particles and the heavier palladium atoms bound together within the lattice. Thus, most of the released kinetic energy will stay inside the core, in the form of additional kinetic energy of the ^{2}D atoms. If the conditions inside the core are right, the reaction can then maintain its own reaction with minimal input energy. The goal of the example calculation is to determine if a self-sustained chain reaction can occur within an LENR reactor when the proper conditions exist within the metal lattice core.

There are two requirements for the proper conditions within the lattice of the Pd core. The first is that the density of the ^{2}D fuel within the lattice must be high, preferably over 90% loading. The second condition is that the lattice assists in the reduction/mitigation of the electronic stopping phenomenon. The reasoning and rationalization of this second condition is explained in Section 2.2.

For these example calculations, the palladium core has a volume of 1 cm^3. The shape of the palladium core is made first into a flat foil. This flat foil is then rolled up, like a rolled-up rug, into a cylinder shape. Furthermore, the cylinder is not wound up as tightly as possible, but rather it is loosely wound, to allow a slight bit of a gap for electrolyte in between the layers of the wound-up foil. This shape is optimum, as it reduces the number of neutrons that can escape the palladium core, and it is similar to the way that fission reactors are designed to optimize the containment of the neutrons. If a neutron escapes one surface of the rolled-up palladium foil, it goes into that slight bit of electrolyte between the layers, is slowed down slightly, and then reenters another part of that wound-up palladium foil.

When palladium metal sample absorbs deuterium, the volume of the sample expands, typically about 20% for a fully-loaded sample of palladium. Thus, when the 1 cm^3 volume of Pd is loaded, it acquires a new volume of 1.2 cm^3. The other parameters of this example calculation are listed in Table 1. These are typical and reasonable values for a typical electrolytic LENR reactor.

Table 1. Parameters of the Example Calculation

Parameter	Value
Volume of unloaded Pd, in cm^3	2.0
Height of cylinder in cm	8.0
Thickness of foil in cm	0.01
gap between the layers of the wound-up foil in cm	0.01
Radius of loosely wound-up cylinder, in cm	0.618
Density of Pd before loading, in atoms/cm 3	$6.80\mathrm{E}+22$
Expansion of Pd core volume when loaded	20%
Volume of loaded Pd core in cm^3 =	1.20
Density of Pd atoms after loading, in atoms/cm 3	$5.670\mathrm{E}+22$
Deuterium loading ratio in the Pd lattice	0.95
Density of D-2 in loaded lattice, in #/cm 3	$5.387\mathrm{E}+22$
Summed output power of the two primary reactions	$1.71\mathrm{E}+12$
b-max-effective for lattice, in m	$3.93\mathrm{E}-07$

Using this table, we can find the total density, in units of number per cm^3, of the palladium and the deuterons in the lattice. The density of palladium is 12.023 gm/cm^3. The atomic weight of palladium is 106.42 for naturally occurring palladium. Thus, one mole of palladium is 106.42 grams, and it contains Avogadro's number of palladium atoms, which is 6.022×10^{23}. As a result, for one cubic centimeter of palladium, there are (106.23 gm/mole)/(12.023 grams) = 0.133 moles, which is (0.113 moles)*(6.022×10^{23} atoms per mole) = 6.804×10^{22} atoms per cm^3. If the palladium expands by 20% when it is loaded, then the loaded volume becomes 1.2 cm^3, and the density of the sample is $6.804 \times 10^{22}/1.2 = 5.67 \times 10^{22}$ atoms/cm^3. If the deuterons are loaded with a 95% ratio of deuterons per palladium atoms, then the density of the deuterons inside the lattice is (0.95)*(5.67×10^{22}) = 5.387×10^{22} per cm^3. Thus, for our example, the total density of the ^{2}D in the lattice is 5.387×10^{22} of ^{2}D per cm^3.

For our example calculation, we assume the reactor is already running with one watt of power, generated by the sum-total of the two primary reactions. Our goal is to see if the reactor can produce and maintain a subsequent chain reaction from this starting point of one watt from the primary reactions. Table 2 shows the energy output of the four reactions [13].

The two primary reactions occur at 50% branching ratio. The energy from the Primary1 reaction is 4.04 MeV, and the energy from the Primary2 reaction is 3.27 MeV. This is an average of 3.655 MeV for every ^{2}D+^{2}D reaction. One watt of power is 6.242×10^{12} MeV/second. Thus, for one watt of power, the number of reactions is (6.242×10^{12} MeV/second)/(3.655) = 1.71×10^{12} reactions per second of the ^{2}D + ^{2}D reaction. This is 8.55×10^{11} reactions per second of each of the two primary reactions.

1.1. Description of the Four-Part Calculation

This is a detailed and complicated calculation, done in four parts. During these calculations, a determination is made for the number of cold ^{2}D that are scattered, and hence energized, by the hot child products of the primary reactions. These same hot primary child products may also react in the secondary reactions with the ^{2}D. For these secondary reactions, those reaction rates are calculated. More child products are produced by these secondary reactions. The number of ^{2}D that are scattered and energized by the hot secondary child products is determined. If there are enough scattered and energized ^{2}D, and if these newly-energized ^{2}D have sufficient kinetic energy to overcome the coulomb barrier, then a subsequent ^{2}D to ^{2}D reaction could occur. The reaction rate of this subsequent ^{2}D to ^{2}D reaction is calculated, and a determination is made as to whether a chain reaction can occur within the reactor.

Table 2. Energies of the primary and secondary reactions.

A	B	C	D	E	F	G	H	J	K
Reaction type and reaction identifier	Nuclide A	Density of nuclide A per cm^3	Nuclide B	Fusion rate in #/sec/cm^3	Child Product A	Child Product B	Energy per reaction, in MeV	Energy of Child Product A after reaction	Energy of Child Product B after reaction
Primary 1 $^2\mathrm{D}+{}^2\mathrm{D}-{}^3\mathrm{T}+\mathrm{p}$	^{2}D cold	5.39E+22	^{2}D hot	8.55E+11	^3T	p	4.04	1.01	3.03
Primary 2 $^2\mathrm{D}+{}^2\mathrm{D}->{}^3\mathrm{He}+\mathrm{n}$	^{2}D cold	5.39E+22	^{2}D hot	8.55E+11	^{3}He	n	3.27	0.8175	2.4525
Secondary 1 $^2\mathrm{D}+{}^3\mathrm{T}->{}^4\mathrm{He}+\mathrm{n}$	^{2}D cold	5.39E+22	^{3}T hot	8.55E+11	^{4}He	n	17.59	3.518	14.072
Secondary 2 $^2\mathrm{D}+{}^3\mathrm{He}->{}^4\mathrm{He}+\mathrm{p}$	^{2}D cold	5.39E+22	^{3}He hot	8.55E+11	^{4}He	p	18.40	3.680	14.720

This four-part example calculation extends through Sections II through V of this paper, as follows.

Section 2: Scattering of child products from the two primary reactions
2.1 A brief overview of nuclear particle scattering for charged particles
2.2 The Unusual Behaviors of Palladium Hydrides and Their Possible Effects on the Scatter Rates
2.3 Calculate the scattering rate of energetic protons with ^{2}D.
2.4 Calculate the scattering rate of energetic ^{3}T with ^{2}D.
2.5 Calculate the scattering rate of energetic ^{3}He with ^{2}D.
2.6 Calculate the scattering rate of energetic neutrons with ^{2}D, using neutron scattering.
2.7 Summary of Section 2.
Section 3: Reaction rate of primary child products
3.1 A brief review of the reaction rate calculations.
3.2 Calculate the reaction rate of the secondary1 reaction, $^3\mathrm{T}+{}^2\mathrm{D}->{}^4\mathrm{He}+\mathrm{n}$.
3.3 Calculate the reaction rate of the secondary2 reaction, $^3\mathrm{He}+{}^2\mathrm{D}->{}^4\mathrm{He}+\mathrm{p}$.
3.4 Summary of section 3.
Section 4: Scattering of child products from the two secondary reactions
4.1 Calculate collision rate of energetic ^{4}He (from secondary1 reaction) with ^{2}D.
4.2 Calculate collision rate of energetic neutrons (from secondary1 reaction) with ^{2}D.
4.3 Calculate collision rate of energetic ^{4}He (from secondary2 reaction) with ^{2}D.
4.4 Calculate collision rate of energetic protons (from secondary2 reaction) with ^{2}D.
4.5 Summary of section 4.
Section 5: Subsequent ^{2}D to ^{2}D reaction and determination of chain reaction
5.1 Add up the energetic ^{2}D in the reactor core from all of the eight child products.
5.2 Calculate the reaction rate for this subsequent ^{2}D to ^{2}D reaction.
5.3 Determine if a chain reaction can occur.
5.4 Summary of section 5.
Section 6: Conclusions.

6.1 Conclusions.

After the four-part example calculations are made in Sections 2-5, the conclusions are discussed in Section 6. The estimates of the expected neutron and gamma ray emissions from the reactor apparatus, involving tertiary reactions, are made in a companion paper, "A Semi-Conventional Explanation for LENR, Part II". Also in this companion paper, the issues regarding electron stopping and the effective impact parameter are discussed, examined, and mathematically estimated.

2. Scattering of Child Products From the Two Primary Reactions

2.1. A Brief Overview of Nuclear Particle Scattering for Charged Particles

2.1.1. *Understanding Electric Elastic Scattering*

The two primary reactions are: ^{2}D+^{2}D−>^{3}T+p and ^{2}D+^{2}D−>^{3}He+n. To begin with this calculation, we need to know how many of these energetic child product projectiles scatter with another ^{2}D inside the core. The energetic child products must scatter a sufficiently large number of ^{2}D, with a sufficiently high enough energy to overcome the coulomb barrier. If so, then a subsequent ^{2}D+^{2}D reaction can occur.

In electric elastic scattering, (aka Rutherford Scattering) three parameters for both the projectile and target must be known: the initial energy, the mass, and the electric charge. Three more parameters must be known, the distance L travelled by the projectile, the density ρ_t of the target particles, and the scattering cross section σ_{scatter}. With these parameters for elastic scattering, the number of scattered particles, and their average energy, can then be determined. The calculations must done be in the center-of-mass reference frame. Some reference sources for this information are here [14], [15], [16].

2.1.2. *Understanding Center-of-Mass Reference Frame*

The center-of-mass angle is related to the lab angle, as shown in Eq. (1).

$$\begin{aligned}\mathrm{Cos}\left(\Theta_{\mathrm{CM}}\right) = {} & \left(\frac{-m_p}{m_t}\right) \times \left(\mathrm{Sin}^2\left(\theta_{\mathrm{LAB}}\right)\right) \\ & \pm \left[\left(\left(\left(\frac{m_p}{m_t}\right)^2\right) \times \left(\mathrm{Sin}^4\left(\theta_{\mathrm{LAB}}\right)\right) - \left(\left(\frac{m_p}{m_t}\right)^2\right) \times \left(\mathrm{Sin}^2\left(\theta_{\mathrm{LAB}}\right)\right) + \mathrm{Cos}^2\left(\theta_{\mathrm{LAB}}\right)\right)\right]^{1/2} \qquad (1)\end{aligned}$$

where:

Θ_{CM} is the deflection angle of the projectile in the center-of-mass reference frame.
θ_{LAB} is the deflection angle of the projectile in the lab reference frame.
m_p is the mass of the projectile
m_t is the mass of the target

Also, for clarification, these variables are defined here.

v_{pi_lab} is the projectile initial velocity in the lab reference frame.
v_{ti_lab} is the target initial velocity in the lab reference frame.
v_{pf_lab} is the projectile final velocity in the lab reference frame.
v_{tf_lab} is the target final velocity in the lab reference frame.
v_{pi_CM} is the projectile initial velocity in the center-of-mass reference frame.
v_{ti_CM} is the target initial velocity in the center-of-mass reference frame.
v_{pf_CM} is the projectile final velocity in the center-of-mass reference frame.

v_{tf_CM} is the target final velocity in the center-of-mass reference frame.
v_{CM} is the velocity of the center of mass.
μ is the reduced mass $= (m_p m_t)/(m_p + m_t)$
For the initial condition of $v_{ti\_lab} = 0$, the equation for the velocity of the center of mass, v_{CM}, is shown in Eq. (2):

$$v_{\mathrm{CM}} = \frac{m_p}{m_p+m_t} v_{pi\_lab} \tag{2}$$

The velocities in of the center-of-mass frame, are shown in Eqs. (3).

$$\begin{aligned} v_{pi\_CM} &= v_{pi\_lab} - v_{\mathrm{CM}} \\ v_{ti\_CM} &= v_{ti\_lab} - v_{\mathrm{CM}} \\ \mathrm{v}_{pi\_CM} &= \left({}^{m_t}/{}_{m_p}\right) v_{ti\_CM} \\ \mathrm{v}_{pf\_CM} &= \left({}^{m_t}/{}_{m_p}\right) v_{tf\_CM} \end{aligned} \tag{3}$$

The initial velocities in the center-of-mass reference frame can be calculated from the laboratory reference frames, using Eqs. (4).

$$\begin{aligned} v_{pi\_CM} &= \left(\frac{m_t}{m_p+m_t}\right) v_{pi\_lab} \\ v_{ti\_CM} &= \left(\frac{m_p}{m_p+m_t}\right) v_{pi\_lab} \\ \mathrm{v}_{pf\_CM} &= \left(\frac{-m_t}{m_p+m_t}\right) v_{pi\_lab} = -v_{pi\_CM} \\ \mathrm{v}_{tf\_CM} &= \left(\frac{-m_p}{m_p+m_t}\right) v_{pi\_lab} = -v_{ti\_CM} \end{aligned} \tag{4}$$

Notice that these Eqs. (4) are all related to the laboratory initial projectile velocity, v_{pi_LAB}. They are related to only v_{pi_LAB} because the laboratory initial target velocity v_{ti_LAB} is assumed to be zero. For the high energy projectiles involved in LENR, we can make the approximation that the velocity of the projectile is much larger than the velocity of the target, $v_{pi\_lab} >> v_{ti\_lab}$.

In the center-of-mass frame, the center-of-mass speeds of the projectile and target do not change as a result of the elastic collision. In other words, if the collision is elastic, then the before and after speeds of the projectile and target are the same, *in the center-of-mass reference frame*. Expressed mathematically, this means: $v_{pf\text{-}CM} = v_{pi\text{-}CM}$, $v_{tf\text{-}CM} = v_{ti\text{-}CM}$.

Also, the velocity of the center of mass does not change. Mathematically, this means: $v_{CM\text{-initial}} = v_{CM\text{-final.}}$ For an elastic collision, this also means that the *initial* relative center-of-mass energy and the *final* relative center-of-mass energy are equal.

If the velocities in the lab reference frame are known for the projectile and target before the collision, v_{pi_lab} and v_{ti_lab}, then the kinetic energies associated with the two particles are known. The total kinetic energy of the system is the sum of the two energies. If the target is assumed to have zero kinetic energy (a reasonable approximation), then this simplifies the total energy of the system in the lab reference frame, E_{total_lab}, as shown in Eq. (5).

$$E_{total\_lab} = \frac{1}{2} m_p v_{p\_lab}^2 \tag{5}$$

The kinetic energy of the center of mass, E_{of_CM}, is simply the energy associated with the motion of the center-of-mass relative to the lab reference frame, as in Eq. (6).

$$E_{of\_CM} = \frac{1}{2}\left(m_p{+}m_t\right)v_{\mathrm{CM}}^2 \tag{6}$$

This energy of the center of mass should not be confused with the particle energies *within* the center-of-mass reference frame. This energy of the center-of-mass does not change as a result of the elastic collision. Also, the velocity, momentum, and kinetic energy of the center-of-mass are conserved throughout the collision. The energy associated with the motion of the center-of-mass does not participate as part of the energy for the collision. In other words, for a collision, this energy *of* the center-of-mass does not aid in overcoming the coulomb barrier. Only the relative energy—the energy *within* the center-of-mass reference frame—is useful in overcoming the coulomb barrier.

The total kinetic energy in the lab reference frame, E_{total_lab}, and the kinetic energy of the center of mass, E_{of_CM} have now been defined. The remaining energy is the kinetic energy associated with relative motion of the two particles, within the center-of-mass reference frame. This relative center-of-mass energy is the energy available for the collision, and consequently, it is often called the "collision energy". The equation for this relative center-of-mass energy is shown in Eq. (7)

$$E_{CM\_relative} = \frac{1}{2}\mu v_{\mathrm{relative}}^2 \tag{7}$$

where, μ is the reduced mass of the two particles, $\mu = (m_p m_t)/(m_p{+}m_t)$, and $v_{relative}$ is the relative velocity with respect to each other. In terms of the lab energy, the relative center-of-mass energy is proportional to the lab energy, with a factor that depends on the masses, as shown in Eq. (8).

$$E_{CM\_relative} = \frac{E_{\mathrm{lab}}\left(m_t\right)}{\left(m_p{+}m_t\right)} \tag{8}$$

where the initial lab energy of the target is assumed to be zero.

2.1.3. *The Equations and Concepts for Scattering*

When is Θ_{CM} is known, the equation for θ_{LAB} is shown in Eq. (9):

$$\mathrm{Tan}\left(\theta_{\mathrm{LAB}}\right) = \frac{\mathrm{Sin}\left(\Theta_{\mathrm{CM}}\right)}{\mathrm{Cos}\left(\Theta_{\mathrm{CM}}\right) + \left(\frac{m_p}{m_t}\right)} \tag{9}$$

When Θ_{CM} is known, the final velocity of the projectile in the lab frame is calculated using Eq. (10):

$$\left(\frac{v_{pf\_lab}}{v_{pi\_lab}}\right) = \frac{\left(m_p^2{+}2m_t m_p \mathrm{Cos}\left(\Theta_{\mathrm{CM}}\right) + m_t^2\right)^{1/2}}{\left(m_p{+}m_t\right)} \tag{10}$$

Conservation of momentum and energy are used to solve for the final energy of both the projectile and the target. Combining Eq. (10) with $E = (1/2)mv^2$, we get the ratio of the initial and final energies of the projectile in the lab reference frame, in Eq. (11):

$$\frac{E_{\mathrm{pf}}}{E_{\mathrm{pi}}} = \frac{\left(m_p^2{+}2m_t m_p \mathrm{Cos}\left(\Theta_{\mathrm{CM}}\right) + m_t^2\right)}{\left(m_p{+}m_t\right)^2} \tag{11}$$

where:

E_{pf} is the final energy of the projectile after the collision in the lab reference frame

E_{pi} is the initial energy of the projectile before the collision in the lab reference frame.

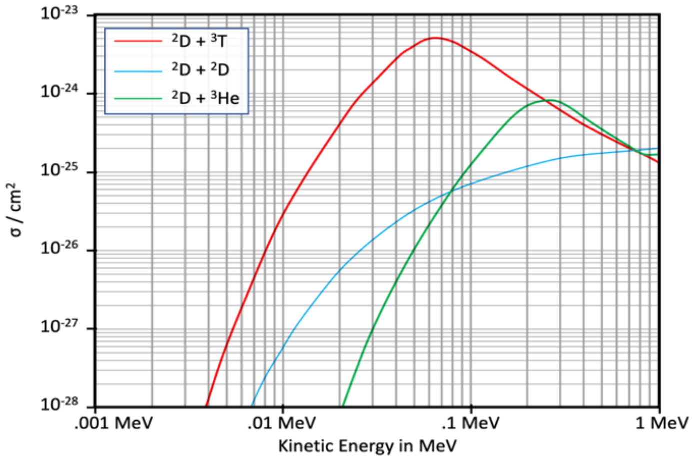

Figure 1. Cross sections of three reactions versus center-of-mass kinetic energy. The chosen threshold value for the ^{2}D+^{2}D reaction is indicated with the blue arrow.

Although the angle used in this equation is the angle from the center-of-mass reference frame, this is the kinetic energy as measured in the lab reference frame. To convert the energy from the lab reference frame to the center-of-mass reference frame, Eq. (8) is used (previously shown.)

Also note, the energy in the lab reference frame depends on which particle is the projectile (defined as the particle having the large kinetic incident energy) and which particle is the target (defined as the particle having approximately zero kinetic energy.) For example, if the projectile is a ^{3}T ion with 1 MeV of kinetic energy, and it is incident upon a target of ^{2}D ion with no kinetic energy, the resulting center-of-mass energy is 0.4 MeV. However, if the projectile is a ^{2}D ion with 1 MeV of kinetic energy, and it is incident upon a target of ^{3}T ion with no kinetic energy, the resulting center-of-mass energy is 0.6 MeV. This is why the center-of-mass reference frame is normally used for the cross-section diagrams, to avoid any ambiguity of which particle is the incident particle.

For an elastic collision, conservation of energy requires that the final energy of the target is the difference between the initial and final energies of the projectile. This is shown in Eq. (12) below.

$$E_{\mathrm{tf}} = E_{\mathrm{pi}} - E_{\mathrm{pf}} \tag{12}$$

In our example, the energetic projectile needs to impart enough energy to a cold ^{2}D, enough to have a possible subsequent reaction.

By looking at the cross-section graph of the ^{2}D to ^{2}D reaction, we select a threshold value where the cross section is large enough to matter, approximately a value of 0.1 MeV of energy. Below that, there will not be much probability of a nuclear reaction; above that value, the cross section is worth considering. We will call 0.1 MeV for a ^{2}D ion to be the "threshold energy".

If the collision between the projectile and the target results in a transfer of 0.1 MeV or more of kinetic energy from the projectile to the ^{2}D target, we will call this a "successful collision", AKA a "successful scattering event". This nomenclature is used throughout the rest of this paper.

Using the threshold energy for successful collision of at least 0.1 MeV to the target, the scattering angle required for a successful scattering event can then be determined. The angle is the lowest angle for which the transferred energy is greater than or equal to 0.1 MeV. Given the initial energy of the projectile and the requirement that $E_{target\_f} \geq 0.1$

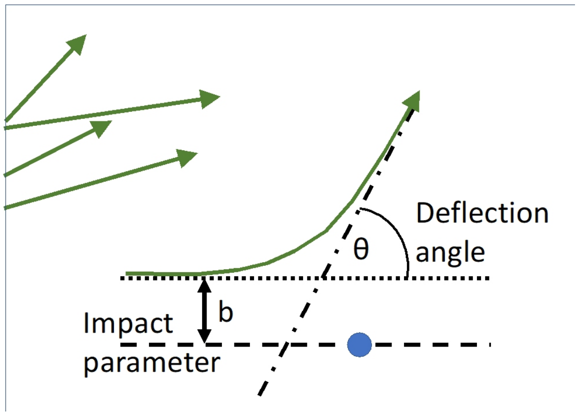

Figure 2. Diagram of scattering impact parameter b.

MeV, the required scattering angle can be determined. With that, we can then determine what fraction of the energetic protons will actually scatter with a ^{2}D, to result in a successful collision.

For the scattering of two charged particles, the impact parameter b is the distance between the trajectory path and the target, shown in Figure 2. The blue dot is the target, and the green arrows are the path of the various projectiles.

The equation for the impact parameter b is shown in Eq. (13).

$$b = \frac{(k)(Z_p)(Z_t)(e^2)}{(2)(E_{total\_CM})} \times \left(\frac{1}{\mathrm{Tan}\left(\frac{\Theta_{\mathrm{CM}}}{2}\right)} \right) \tag{13}$$

where:

Z_p is the number of protons in the projectile

Z_t is the number of protons in the target

k is Coulomb's constant, which is 8.99×10^9 in MKS units.

e is the elementary charge of a proton of 1.602×10^{-19} coulombs in MKS units.

Θ_{CM} is the scattering angle of the projectile in the center-of-mass reference frame.

E_{total_CM} is the sum total energy of the two projectiles in the center-of-mass reference frame.

Note that E_{total_CM} is sometimes called the relative center-of-mass energy, and is shown in Eq. 14:

$$E_{total\_CM} = \frac{1}{2}(\mu)(v_{relative\_CM})^2 \tag{14}$$

where:

μ is the reduced mass, $(m_p m_t)/(m_p+m_t)$

$v_{relative\_CM}$ is the initial relative velocity of the particles in the center-of-mass frame.

The initial relative velocity is the difference between the initial projectile and target velocities, $v_{relative\_CM} = v_{pi\_lab} - v_{ti\_lab}$. However, since it is assumed that the initial target velocity is zero, $v_{ti\_lab} = 0$, this gives the relative velocity of the particles in the center-of-mass frame as equal to the initial projectile velocity in the lab frame. Mathematically, this means $v_{relative\_CM} = v_{pi\_lab}$.

The total kinetic energy in the center-of-mass reference frame can also be written as the sum of the kinetic energies of the particles, using the center-of-mass velocities, shown in Eq. (15).

$$E_{total\_CM} = \frac{1}{2}m_p\left(v_{pi\_CM}\right)^2 + \frac{1}{2}m_t\left(v_{ti\_CM}\right)^2 \tag{15}$$

This is just another way to write it, and it is mathematically equivalent to Eq. (14).

As seen in Eq. (13), the center-of-mass deflection angle Θ_{CM} and the impact parameter b are related—with larger deflection angles occurring for smaller impact parameters. The scattering cross section for a given impact parameter is simply the area of a circle of radius b, shown below in Eq. (18):

$$\sigma = \pi b^2 \tag{18}$$

Combining Eqs. (13), (14) and (18) gives the scattering cross section as shown in Eq. (19):

$$\sigma = \pi\left(\frac{(k)(Z_p)(Z_t)(e^2)}{(\mu)(v_{\text{pi}}^2)}\right)^2\left(\frac{1}{\left(\frac{\Theta_{\text{CM}}}{2}\right)}\right) \tag{19}$$

An important point to make here is that this scattering cross section, σ, is an area not only for scattering events with an impact parameter equal to b, but also for any scattering event with an impact parameter smaller than b. Therefore, the cross section in Eq. (19) is the cross section for any scattering event with a deflection angle that is equal to or greater than the center-of-mass deflection angle, Θ_{CM}. To reiterate this important point—for a given scattering cross section, the center-of-mass deflection angle has a range of values, equal to or greater than Θ_{CM}.

The goals of this example calculation are to find the number of successful scattering events, as well as the average energy of these successful scattering events. For these two goals, both the probability function, P(Θ_{CM}), and the energy E(Θ_{CM}) as a function of that angle, must be known.

The probability function of a scatter, occurring at or greater than an angle Θ_{CM}, is proportional to the cross section, as shown in Eq. (20).

$$P\left(\Theta_{\text{CM}}\right) \propto \sigma \tag{20}$$

The cross section σ shown in Eq. (19) is the scattering cross section for any angle equal to or greater than Θ_{CM}. Thus, the scattering cross section for only one angle is the scattering cross section at one angle, Θ_{CM}, minus the cross section for a slightly larger angle, $\Theta_{CM}+\Delta\Theta_{CM}$. Combining this with Eq. (19), the non-normalized probability function P(Θ_{CM}) is shown in Eq. (21).

$$P\left(\Theta_{\text{CM}}\right) = \left(\frac{\pi\rho \text{L} N_{\text{Avog}}}{A \times 0.001}\right)\left(\frac{kZ_pZ_te^2}{\mu v_{\text{pi}}^2}\right)^2\left[\left(\frac{1}{\left(\frac{\Theta_{\text{CM}}}{2}\right)}\right) - \left(\frac{1}{\left(\frac{\Theta_{\text{CM}}+\Delta\Theta_{\text{CM}}}{2}\right)}\right)\right] \tag{21}$$

To determine the expectation value of the projectile final energy $E_{expect\_pf,}$ the energy is multiplied by the probability, and then integrated over the entire range of possible Θ_{CM}. This is divided by the integral of the probability function, to normalize the function, as shown in Eq. (22).

$$E_{expect\_pf} = \frac{\int P\left(\Theta_{\text{CM}}\right) E(\Theta_{\text{CM}})d\Theta_{\text{CM}}}{\int P(\Theta_{\text{CM}})d\Theta_{\text{CM}}} \tag{22}$$

Substituting Eqs. (11) and (21) into Eq. (22), and solving for the ratio of $E_{\text{expect\_pf}}/E_{\text{ip}}$, results in Eq. (23).

$$E_{\text{expect}_{\text{pf}}} == \frac{\int\left[\left(\frac{1}{\left(\frac{\Theta_{\text{CM}}}{2}\right)} - \frac{1}{\left(\frac{\Theta_{\text{CM}}-1^\circ}{2}\right)}\right)E_{\text{ip}}\left(\frac{\left(m_p^2+2m_tm_p\text{Cos}(\Theta_{\text{CM}})+m_t^2\right)}{(m_p+m_t)^2}\right)d\Theta_{\text{CM}}\right]}{\int\left[\left(\frac{1}{\left(\frac{\Theta_{\text{CM}}}{2}\right)} - \frac{1}{\left(\frac{\Theta_{\text{CM}}-1^\circ}{2}\right)}\right)d\Theta_{\text{CM}}\right]} \tag{23}$$

With this formula, we now have the ability to find the average final energy for the average projectile as it scatters with the target. These integrals can be solved with numerically, which converts the integrals into summations, as shown in Eq. (24).

$$E_{expect\_pf} = \frac{\sum_{i=\Theta_{CM\_min}}^{\Theta_{CM\_max}} \left[\left(\frac{1}{\mathrm{Tan}^2\left(\frac{\Theta_{CM\_i}}{2}\right)} - \frac{1}{\mathrm{Tan}^2\left(\frac{\Theta_{CM\_i}-\Delta\Theta_{CM\_i}}{2}\right)}\right) E_{\mathrm{ip}} \left(\frac{\left(m_p^2+2m_t m_p \mathrm{Cos}(\Theta_{\mathrm{CM}})+m_t^2\right)}{(m_t+m_p)^2}\right)\Delta\Theta_{CM\_i}\right]}{\sum_{i=\Theta_{CM\_min}}^{\Theta_{CM\_max}} \left[\left(\frac{1}{\mathrm{Tan}^2\left(\frac{\Theta_{CM\_i}}{2}\right)} - \frac{1}{\mathrm{Tan}^2\left(\frac{\Theta_{CM\_i}-\Delta\Theta_{CM\_i}}{2}\right)}\right)\Delta\Theta_{CM\_i}\right]} \tag{24}$$

Given this equation (24), the expectation value for the final energy can be found for a given initial energy, E_{ip}. The projectiles will scatter more than once, giving up a small fraction of their energy to the targets with each scatter. Thus, in order to calculate the energies of the projectiles as they slow down, the calculations of Eq. (24) must be repeated for each initial energy prior to the scatter. Thus, we need to consider all of the scattering events as the projectile loses its energy—from the original energy of the projectile, $E_{\mathrm{ip\_original}}$, down to the threshold energy of 0.1 MeV. To do this, ideally, an integration over E_{ip} would be performed, as shown in Eq. (25).

$$E_{expect\_pf\_total} = \int_{0.1}^{E_{ip\_original}} \left(E_{expect\_pf}\right) \mathrm{d}E_{\mathrm{ip}} \tag{25}$$

However, rather than an integration, this will instead be done using summations and discrete steps in the energy range, shown in Eq. (26)

$$E_{expect\_pf\_total} = \sum_{E_{\mathrm{ip}}=0.1}^{E_{ip\_original}} \left(\frac{\sum_{i=\Theta_{CM\_min}}^{\Theta_{CM\_max}} \left[\begin{array}{c}\left(\frac{1}{\mathrm{Tan}^2\left(\frac{\Theta_{CM\_i}}{2}\right)} - \frac{1}{\mathrm{Tan}^2\left(\frac{\Theta_{CM\_i}+\Delta\Theta_{CM\_i}}{2}\right)}\right) \\ E_{\mathrm{ip}}\left(\frac{\left(m_p^2+2m_t m_o \mathrm{Cos}(\Theta_{\mathrm{CM}})+m_t^2\right)}{(m_t+m_p)^2}\right)\Delta\Theta_{CM\_i}\end{array}\right]}{\sum_{i=\Theta_{CM\_min}}^{\Theta_{CM\_max}} \left[\left(\frac{1}{\mathrm{Tan}^2\left(\frac{\Theta_{CM\_i}}{2}\right)} - \frac{1}{\mathrm{Tan}^2\left(\frac{\Theta_{CM\_i}+\Delta\Theta_{CM\_i}}{2}\right)}\right)\Delta\Theta_{CM\_i}\right]} \right) \tag{26}$$

As the energy of the projectile steps down, from one range to a lower range, the minimum scattering angle Θ_{CM_min} changes as well. Thus, we must redo the calculation for Θ_{CM_min} each energy range, and use the appropriate value of Θ_{CM_min}. The results are summed to find $E_{\mathrm{expect\_pf\_total}}$.

2.1.4. *Finding the Average Target Energy of the Successful Scattering Events*

To find the average energy of the projectiles of only the successful scattering events Eq. (26) is again used, but with the lower integration limit of the numerator changed to $\Theta_{success}$. Thus, when Eq. (26) is calculated between the limits of $\Theta_{CM\_success}$ to Θ_{CM_max}, the expectation energy for only the successful scattering events is found. The target energy is then found with Eq. (12). The first goal of finding the mean energy value of the successfully scattered targets is then achieved.

2.1.5. *Finding the Number of the Successful Scattering Events*

The second goal is to find the number of successful scattering events. The probability equations can also give us this fraction of successful scattering events. The fraction of successful scatters, $\mathrm{fraction}_{\mathrm{successful}}$, is found by using the successful scattering angle, $\Theta_{CM\_success}$ and then summing that probability for all angles equal to or greater than the successful scattering angle. That sum is then divided by the total probability for all angles, to normalize it. This is shown in Eq. (27).

$$\text{fraction}_{\text{successful}} = \frac{\sum_{i=\Theta_{CM\_success}}^{\Theta_{CM\_max}} \left[\left(\frac{1}{\text{Tan}^2\left(\frac{\Theta_{CM\_i}}{2}\right)} - \frac{1}{\text{Tan}^2\left(\frac{\Theta_{CM\_i}+\Delta\Theta_{CM\_i}}{2}\right)} \right) \Delta\Theta_{CM\_i} \right]}{\sum_{i=\Theta_{CM\_min}}^{\Theta_{CM\_max}} \left[\left(\frac{1}{\text{Tan}^2\left(\frac{\Theta_{CM\_i}}{2}\right)} - \frac{1}{\text{Tan}^2\left(\frac{\Theta_{CM\_i}+\Delta\Theta_{CM\_i}}{2}\right)} \right) \Delta\Theta_{CM\_i} \right]} \tag{27}$$

As before, this function for $fraction_{successful}$ needs to be done for each energy range, going from the original energy of the energetic child particle, all the way down to 0.1 MeV. The results are summed.

2.1.6. *Finding the Integration Limits*

What is left to determine are the maximum scattering angle, the minimum scattering angle, and successful scattering angle. In the center-of-mass reference frame, Θ_{CM_max} is always 180°.

To find the Θ_{CM_min} we must first find the maximum impact parameter, b_{max}.

In a lattice, this is a difficult question. However, in a plasma, wherein the deuterium fuel is ionized and free to move about, this can be easily solved. For a plasma, the maximum impact parameter b_{max} would be dependent upon the density of the ^{2}D in the plasma. The reciprocal of this density is the average volume per deuteron particle. The *average* distance between two deuteron ions would be the cube root of that. If the projectile travels halfway between two deuterons, this is the maximum distance, on average, that a projectile could be from any given deuteron. This is the maximum impact parameter, b_{max}, that could occur within the plasma, as shown in Eq. (28), where $\rho_{deuteron}$ is the plasma density of the ^{2}D, in number of deuterons ion per cm^3.

$$b_{\max} = \left(\frac{1}{2}\right) \sqrt[3]{\frac{1}{(\rho_{\text{deuteron}})}} \tag{28}$$

This value of b_{max} is the maximum impact parameter. (See Figure 2). It is the distance between a projectile trajectory and target. The main loss of energy, in a plasma, is the loss of the ionic kinetic energy to the electrons within the plasma, known as braking radiation, or Bremsstrahlung. For a plasma, this is a significant energy loss.

Using this estimated value for b_{max}, we can insert it into Eq. (17), and solve for $\Theta_{CM\_min.}$ This is shown in Eq. (29).

$$\Theta_{CM\_min} = 2 \times ArcCot \left[\left(\frac{m_p m_t}{m_p + m_t} \right) \times \left(\frac{b_{\max} v_{\text{pi}}^2}{ke^2 Z_p Z_t} \right) \right] \tag{29}$$

The initial projectile velocity v_{pi} depends on the energy and mass of the projectile. Thus, this calculation needs to be done not only for each projectile, but also for also for every energy range of the projectile.

The successful scattering angle, $\Theta_{CM\_success}$, is found by solving Eq. (11) for $\Theta_{CM\_success}$. This gives us Eq. (30), shown below.

$$\Theta_{CM\_success} = ArcCos \left[\frac{\frac{E_{pf\_success}}{E_{\text{pi}}} (m_p + m_t)^2 - m_p^2 - m_t^2}{(2 m_p m_t)} \right] \tag{30}$$

where E_{pi} is the initial energy of the projectile, and $E_{pf\_success}$ is the final energy of a successful scattering event. (Note that the impact parameter b is not a term in this equation.) For the successful scatter, E_{tf} is at least 0.1 MeV of energy. Thus, $E_{\text{pf\_success}}$, is defined by $E_{\text{pf\_success}} = E_{\text{pi}} - 0.1$ MeV. Using $E_{pf\_success}$ in Eq. (30) yields the threshold successful angle $\Theta_{CM\_success}$ required for a successful scattering event. The values of Θ_{CM} that are equal to or larger than $\Theta_{CM\_success}$ result in a successful scattering event. The value of $\Theta_{CM\_success}$ is dependent on a collection of constants and the energy of the energetic ion, thus there is very little that can be done in the design of the reactor to change this value.

With these equations, and the values for the integration limits, we can now determine the number and average energy of the successfully scattered ^{2}D targets for one energy range of the projectile. This process must be repeated for each energy range of the projectile, from its original energy down to 0.1 MeV. The results are summed.

A sample calculation of the numeric integration is done here, to demonstrate the mathematics and formulas used. The integration limits are from Θ_{CM_min} to Θ_{CM_max}. The denominator of Eq. (27) is shown in Eq. (31), for one value of Θ_{CM}.

$$P_i\left(\Theta_{\text{CM}}\right) \propto \left[\left(\frac{1}{\text{Tan}^2\left(\frac{\Theta_{CM_i}}{2}\right)} - \frac{1}{\text{Tan}^2\left(\frac{\Theta_{CM_i}+\Delta\Theta_{\text{CM}}}{2}\right)}\right)\right] \tag{31}$$

Inserting numbers in this, with $\Theta_{CM\_i} = 0.001°$, $\Delta\Theta_{CM} = 0.001°$, a value proportional to $P(\Theta_{CM})$ is shown in Calc. 1.

$$P\left(\Theta_{\text{CM}}\right) \propto \left[\left(\frac{1}{\text{Tan}^2\left(\frac{0.0001°}{2}\right)} - \frac{1}{\text{Tan}^2\left(\frac{0.0002°}{2}\right)}\right)\right] = 9.8484 \times 10^{11} \qquad \text{(Calc. 1)}$$

This value is the non-normalized probability function, as seen in Table 3, first row column E. This calculation is repeated out to 180°. (For simplicity, Table 3 only shows a few sample rows of the actual table, which is extremely large for the numerical integration. Also, the actual table starts with a smaller angle.) Columns A and B show the value of Θ_{CM} in both degrees and radians. Column C is the value of $\Delta\Theta_{CM}$ used for the numeric integration. Column D is the probability function $P(\Theta_{CM})$. Column E is the probability function $P(\Theta_{CM})$ times the ratio $E_{\text{pf}}/E_{\text{pi}}$. This value, in Column E, will be used in the summation of the numerator of Eq. (24). The values used in column E of Table 3 are $m_{\text{p}} = 1$, and $m_{\text{t}} = 2$, such as for a proton colliding with a deuteron. (Note that the ratio $E_{\text{pf}}/E_{\text{pi}}$ is very close to one, for these extremely small angles, such that the values in column D and E appear to be the same. However these values do vary for the larger angles, as can be seen in the last row.)

To find the expectation value of energy for only the successful scatters, we sum column E from $\Theta_{CM\_successful}$ to Θ_{CM_max}, as indicated in Eq. (27).

By using the full table, which goes out to 179° for the center-of-mass deflection angle Θ_{CM}, and by selecting the appropriate angles for $\Theta_{CM\_success}$, Θ_{CM_min}, and Θ_{CM_max} within that table, the numerical integrations can be performed for both the probability function, $P(\Theta_{CM})$, and for the probability function times the energy, $P(\Theta_{CM}) \times E_{\text{pf}}(\Theta_{CM})$. Using the results of these numerical integrations, the total expectation energy of the projectiles, for the entire energy range, $E_{\text{expect\_pf\_total}}$, can be found, using Eq. (26).

The values in Table 3 are used for the numeric integration for protons scattering off deuterons. This entire table for numeric integration is recalculated for all of the other types of excited charged projectiles: ^{3}T, ^{3}He, and ^{4}He. However, these very large integration tables are not shown.

The last variable to calculate is the average number of times, N_{ave}, that the projectile scatters. In order to calculate N_{ave}, we first need to know the average fractional energy loss for one collision. This will allow us to determine how much the projectile's energy has decreased, on average, after each collision. This average fractional energy loss is

Table 3. Numeric integration data for protons projectiles on ^{2}D targets, used to find the expectation value of the final projectile energy.

A	B	C	D	E
θ_{CM} in degrees	θ_{CM} in radians	$\Delta\theta_{\mathrm{CM}}$ in radians	Probability $P\left(\Theta_{\mathrm{CM}}\right)$	$P(\theta) \times E_{\mathrm{pf}}(\theta)/E_{\mathrm{pi}}(\theta)$
0.0001	1.745E-06	1.745E-06	9.848E+11	9.848E+11
0.0002	3.491E-06	1.745E-06	1.824E+11	1.824E+11
0.0003	5.236E-06	1.745E-06	6.383E+10	6.383E+10
0.0004	6.981E-06	1.745E-06	2.955E+10	2.955E+10
0.0005	8.727E-06	1.745E-06	1.605E+10	1.605E+10
0.0006	1.047E-05	1.745E-06	9.677E+09	9.677E+09
0.0007	1.222E-05	1.745E-06	6.281E+09	6.281E+09
0.0008	1.396E-05	1.745E-06	4.306E+09	4.306E+09
0.0009	1.571E-05	1.745E-06	3.080E+09	3.080E+09
0.0010	1.745E-05	1.745E-06	2.279E+09	2.279E+09
0.0011	1.920E-05	1.745E-06	1.733E+09	1.733E+09
*	.	.	.	...
179	3.124139	1.745E-02	7.616E-05	8.467E-06

found by using Eq. (24), for one given initial energy E_{pi}, and then calculating the resulting E_{pf}. Then Eq. (32) is used to find the fractional energy_loss. Recall that E_{pf} has already been determined for each energy range.

$$\text{fraction}_{energy\_loss} = \frac{E_{\mathrm{pi}} - E_{\mathrm{pf}}}{E_{\mathrm{pi}}} \tag{32}$$

$$\text{fraction}_{energy\_loss} = 1 - \frac{\sum_{i=\Theta_{CM\_min}}^{\Theta_{CM\_max}} \left[\left(\frac{1}{\mathrm{Tan}^2\left(\frac{\Theta_{CM\_i}}{2}\right)} - \frac{1}{\mathrm{Tan}^2\left(\frac{\Theta_{CM\_i}-\Delta\Theta_{CM\_i}}{2}\right)} \right) \left(\frac{\left(m_p^2 + 2m_t m_p \mathrm{Cos}(\Theta_{\mathrm{CM}}) + m_t^2\right)}{(m_t+m_p)^2} \right) \Delta\Theta_{CM\_i} \right]}{\sum_{i=\Theta_{CM\_min}}^{\Theta_{CM\_max}} \left[\left(\frac{1}{\mathrm{Tan}^2\left(\frac{\Theta_{CM\_i}}{2}\right)} - \frac{1}{\mathrm{Tan}^2\left(\frac{\Theta_{CM\_i}-\Delta\Theta_{CM\_i}}{2}\right)} \right) \Delta\Theta_{CM\_i} \right]}$$

The initial projectile energy cancels out of the equation. Thus with each collision, the average energy of the projectile is reduced by the same average fractional energy loss. The number of collisions is required to reduce the energy of the projectile—from one energy, E_1, to a lower energy E_2—is shown in Eq. (33).

$$\frac{E_2}{E_1} = \left(1 - \text{fractional}_{energy\_loss}\right)^N \tag{33}$$

Solving for N, the average number of collisions, we get Eq. (34):

$$N = \frac{\mathrm{Ln}\left(\frac{E_2}{E_1}\right)}{\mathrm{Ln}\left(1 - \text{Fractional}_{energy\_loss}\right)} \tag{34}$$

At this point, we have discussed all the relevant equations for charged particle scattering.

2.2. The Unusual Behaviors of Palladium Hydrides and Their Possible Effects on the Scatter Rates

Palladium hydride is one of the most-studied interstitial metal hydrides, due to the many unusual, unexplained, and often theoretically-unpredictable changes in its physical behaviors [17]. For example, some of its unusual behaviors include:

- Ordered phases
- Anomalous properties at temperatures below 100 K
- A superabundant-vacancy phase with stoichiometry Pd_3H_4 formed at high temperature and pressure
- Quenching of the enhanced Pauli para-magnetism of palladium
- Superconductivity at 10 K without external pressure
- An inverse isotope effect in its superconductive properties
- An anomaly in the low-temperature specific heat, called the "50-K anomaly".
- Anomalies in resistivity
- Anomalies in the Hall effect
- Anomalies in internal friction
- Thermal expansion
- Ordering of interstitial deuterium.

Other anomalous properties of palladium hydride are as listed below.

- Modern first-principles approaches are unable to predict the superconducting transition temperature.
- Anharmonicity of the hydrogen site potential is a key factor and poses a great challenge, theoretically, to explain its superconducting properties.
- The phonon band structure of palladium hydride is particularly problematic, due to the lack of a realistic treatment of anharmonicity–required to reproduce the results of inelastic neutron scattering experiments.
- PdH and its isotopic hydrides have the highest known T_c values of any metal hydride not subject to extreme hydrostatic pressure.

The structural and thermodynamic properties of the Pd–H_2 system were comprehensively reviewed by Manchester et al. [18].

Many of these unusual phenomena should be understandable from the relationships between the electron band structure, phonon band structure, and crystal structure. However, despite very many experimental and theoretical studies, the most advanced calculation of the superconducting transition temperature was only qualitatively, not quantitatively, correct.

2.2.1. *Complexities of a Lattice*

The calculation, shown in Eq. (28), is not only overly naïve and overly simple, but it is incorrect for a lattice. In a lattice, the situation is much more complex and much more difficult to calculate. This is due to the many electrons that are around the Pd, as well as the conduction band electrons (aka sea electrons), from both the Pd and the ^{2}D. Besides the positive charge of one ion, as in Rutherford scattering model, there are also the hundreds of positively charged nuclei, all with positive electric fields. These nuclei include both the lattice Pd nuclei and the ^{2}D nuclei. These positive nuclei alter the positions and electric fields of the sea electrons. Due to all of these complexities in the lattice, the electric field at any given point is not the simplistic assumptions made in Rutherford scattering–wherein only one projectile ion and one target ion are considered. Thus, scattering is not just a simply calculation involving one ion passing another ion of similar charge. Rather, there are positive and negative charges nuclides on all sides of the target–left, right, front, behind, above and below–all extending throughout the lattice in an array of infinite-like columns and rows. As a result, the Pd atoms are not significantly moved or repulsed as a positively-charged energetic ion passes by.

2.2.2. *Channeling*

Many physical phenomena can occur when a charged ion traverses through a solid target. For example, elastic scattering, inelastic energy-losses, secondary-electron emission, electromagnetic radiation, and nuclear reactions. For charged particles, all of these processes have an interaction or reaction cross section, which depends on the impact parameters involved in collisions with the individual target atoms. When the target material is monocrystalline, as is the case for palladium, the reaction rates of these physical processes are dependent on the orientation of the direction of travel relative to the crystalline axes or planes. In other words, the stopping power of the particle is much lower in certain directions than others. This effect is commonly called the "channeling" effect.

In condensed-matter physics, channeling is the process that constrains the path of a charged particle within a crystalline solid. [19], [20], [21], [22], [23]

When channeling occurs, the ions can travel much further without losing energy to the lattice. In crystalline materials, the ion may get focused into a channel between the crystal planes, where it experiences essentially no collisions with nuclei. Also depending on the energy of the ions, the electronic stopping power may be mitigated within the channel. Thus, the energy loss of the ion to the lattice depends on the material type and material density, and it also depended on the materials microscopic structure.

The channeling effect can be understood as follows: When a charged particle traverses through a monocrystal, if the direction of travel lies close to a major crystal direction, then the particle will only do small-angle scattering as it passes through the several layers of atoms in the crystal. Hence the ion will remain in the same crystal channel. Conversely, if it is in a random direction, it is much more likely to undergo large-angle scattering and as a result its penetration depth would be much shorter. Channeling leads to deeper penetration of the ions in the material, an effect that has been observed experimentally.

Positively charged ions are repelled from the nuclei of the crystalline plane. So positively charged particles tend to follow the direction between two neighboring crystalline planes, but at the largest possible distance from each of them. Therefore, the positively charged particles have a smaller probability of interacting with the nuclei and electrons of the planes, and hence they travel longer distances.

2.2.3. *Projectile Ions Convey Electrons*

Another interesting phenomenon is an effect wherein the projectile ions convey, or transport, electrons. It has been shown that if an ionic projectile is moving through a host lattice, and it is moving slowly enough for electrons to follow it, then this phenomenon occurs, wherein the ion can then transport an electron. The electron is thus in a quasi-bonded state, with it as it travels through the lattice [24].

When the electrons are able to follow the energetic projectile ion, then two benefits are achieved. First, these electrons electrically screen the ion, thereby reducing the ability of the ion to penetrate the electron cloud of the lattice host material, which in turn promotes the channeling effect described above. Second, these electrons reduce the effective Coulomb barrier. This is described in the following quote [25].

> "At normal conditions for a material, its ions move relatively slowly, with characteristic particle thermal and sound velocities in excess of 10^3 m/s, while electrons are relatively fast, with effect Fermi velocity v_F (for valence or conduction electrons) in the order of 10^6 m/s. Naturally, this defines two regimes for the stopping process: One at low velocity, the nuclear stopping regime; in which the charged particle mainly loses energy

through an effective interaction with the host ions (while the electrons respond instantaneously without undergoing noticeable excitations), and another regime at high velocity, the electronic stopping regime; in which the charged particle loses energy by partially screened Coulomb interactions with the electrons while the host ions simply have no time to react due to their large inertia (mass). In both regimes, the charged particle interacts equally with electrons and ions (through Coulomb forces), the main difference is the precise dynamical process involved in the energy loss (screened lattice excitations vs. electronic excitations, respectively)."

In other words, at low ion projectile velocity, the charged projectile ions tend to interact with the nucleus, not the electrons. Only at high ion velocity, do they interact with the electrons. The threshold for this behavior difference is dependent upon how easily the electrons can follow the ion at a given energy. This phenomenon of electron conveyance is related to electron screening,

2.2.4. *Electron Screening*

Experimental data show that electron screening improves the likelihood of a reaction, by as much as is 12 to 20 orders of magnitude [26]. Electron screening results in a more transparent Coulomb Barrier, which shifts the Gamow Factor, and the result is as if deuterons were at far higher energies. Laboratory experiments, using accelerated deuteron beams, show that lattice screening can provide up to 3 keV of screening. This results in higher nuclear reaction rates [8] but only at lower energies, below 10 keV, where the reaction rate is too small to be significant. Thus, electron screening effect does not affect the reaction rates in a considerable manner.

2.2.5. *Magnetic Susceptibility of PdDx*

The term magnetic susceptibility describes the response of the material to an external magnetic field. As a palladium lattice PdDx is loaded with more deuterium, its magnetic susceptibility changes significantly as a function of x, actually going from paramagnetic to diamagnetic [27].

> "Measurements have been made of the magnetic susceptibility of PdH and PdD alloys over the temperature range between 4K and 300K.... For the alpha phase, the susceptibility is large and varies with temperature in a manner similar to that of pure palladium, while the susceptibility of the beta phase is slightly diamagnetic and almost independent of temperature."

The magnetic susceptibility of any material is strongly dependent on the behavior of the electrons in the material. Thus, this change, wherein palladium PdDx goes from paramagnetic to diamagnetic, indicates that the electrons in the PdDx material are concurrently undergoing changes with regards to their spin and magnetic alignment as a function of x.

2.2.6. *Specific Heat Coefficient of PdDx*

Another property of PdD_x that changes significantly as a function of $\times$ is the electronic specific heat coefficient, C_e [28]. For the electronic specific heat coefficient, this is a metallic property that depends on the electron density of states. For pure palladium, it is 9.5 mJ(mol·K2). When hydrogen is added to the Pd, the electronic heat coefficient drops significantly. For the range of $\times = 0.83$ to $\times = 0.88$ the electronic specific heat coefficient is measured to be six times smaller than for pure Pd [28]. This means that with a lower C_e, the electrons do not move around as much as they would with a higher C_e.

To understand how this change in electronic specific heat affects the electronic behavior, consider this quote from reference [29], describing the electronic specific heat of superconductors.

> "The electronic specific heat (C_e) of the electrons is defined as the ratio of that portion of the heat used by the electrons to the rise in temperature of the system."

In other words, if C_e is low, most of the energy is going to the lattice vibration. When C_e is high, then the electrons move around much more, comparatively. Continuing with the same quote:

> "When a small amount of heat is put into a system, some of the energy is used to increase the lattice vibrations (an amount that is the same for a system in the normal and in the superconducting state), and the remainder is used to increase the energy of the conduction electrons."

Thus, if one joule of heat energy is put into a material with a high C_e, the conduction electrons move around more than they would for a material with a low C_e. Continuing with that quote:

> "The electronic specific heat in the superconducting state (designated C_{es}) is smaller than in the normal state (designated C_{en}) at low enough temperatures."

In their superconducting state, superconductors have an extremely low resistivity. As described above, the electrons in a superconducting state have a low electronic specific heat. As a result, when the material is in a superconducting mode, the heat added to the material does not cause the electrons to move around, and they do not have an abundance of kinetic energy. Rather the electrons are essentially moving with little more than the slow motion of the electric current.

This same phenomenon of a low C_e occurs in PdD_x, simply by adding more deuterons into the lattice. The electronic specific heat is lowered by a factor of six, meaning that the electrons are not as easily activated by the introduction of heat. Rather, they are sluggish, just as they are for a superconductor in a superconducting state. Given this condition within the PdD_x lattice, it can be easily posited that the electron stopping process might be beneficially shifted with respect to the ionic stopping, to allow for longer ionic travel distances within the lattice, and thus higher reaction rates.

2.2.7. *Superconductivity of PdDx*

Given this information about ion channeling, convey electrons, and electron screening, coupled with the fact that the electrons in a PdD_x lattice have in increased mobility, some interesting inferences can be made. Experimental evidence implies that superconductors are dominated by nuclear stopping, rather than electron stopping. PdD_x is a superconductor, and its behavior is dependent on the loading ratio x.

Ishikawa et al. found that when low energy projectiles, (less than 2 MeV), traversed through superconducting materials, the defect production rate in the lattice of the superconductor was proportional to the nuclear stopping power, rather than electron stopping [30].

In their experiments on a superconductor, Ishikawa and his team found that for low energy projectiles, the defect production rate is proportional to nuclear stopping power, rather than electron stopping. This can be understood by realizing that the parameter corresponding to the defect production rate has two contributions. The effect via elastic displacement, due to nuclear collisions, and the effect via electronic excitation, due to electron stopping. They found that for low energy ion irradiation, less than 2 MeV, the defect production rate was proportional to the nuclear stopping power, rather than electron stopping. The contribution from electron stopping only became apparent for high ion energies, over 80 MeV. Quoting from their text:

> "For low energy ($\leq$2 MeV) ion irradiation, $(\Delta c/c_0)/\Phi$, which corresponds to the defect production rate, is proportional to the nuclear stopping power, S_n. On the other hand, for high energy (80 MeV$-$3.8 GeV) ion irradiation, the contribution of electronic excitation to $(\Delta c/c_0)/\Phi$ is precisely estimated by assuming that

the observed ($\Delta c/c_0$)/Φ value is the sum of the contribution of elastic displacement and that of electronic excitation."

Other researchers have found similar results when studying superconductive materials. Baubour et al. [31] found that the damage in the lattice of superconductors is created by elastic collisions, which indicates that the nuclear stopping power S_n is the dominant stopping power. Quoting from the text:

> "For ions with energies less than several MeV, the dominant mechanism causing irradiation-induced degradation of Tc is collisional damage."

This agrees with previous experiments [32]:

> "The defect production rate, which is obtained from the initial slope of the resistance–fluence curve, is almost proportional to the nuclear stopping power, S_n. The T_c depression due to irradiation is also nearly proportional to S_n. These results indicate that the defect production process is dominated by elastic displacement. ... In high-T_c superconductor $EuBa_2Cu_3O_y$ irradiated with 2 MeV electrons and 0.5–2.0 MeV ions, the normal-state resistance change and T_c depression due to irradiation are nearly proportional to S_n, indicating that the elastic displacement is a dominant damage production process."

In other words, these other behaviors of the lattice that follow this same trend–that S_n dominates at ion projectile energies below several MeV. For superconducting materials, there is a behavior occurring within the lattice which mitigates the electron stopping power at these energies, (below several MeV).

Let us examine how electronic and nuclear stopping relate to each other. Below is a typical curve of electron stopping power and nuclear stopping power, plotted together, versus ion energy. This is for pure aluminum. At energies of around 1 to 2 MeV, notice that the electron stopping power dominates.

The comparative placement of the two stopping-power curves, relative to each other, is dependent on several factors. For example, here is a similar curve, showing the electron stopping and nuclear stopping for SiO_2 bombarded with Au ions. At ion energies below 2 MeV, the nuclear stopping power dominates.

There are several the unique properties of the PdD_x lattice, that may be mitigating the effects of electron stopping. Here is a list of unusual behaviors and properties of the PdD_x lattice.

- PdD_x is a superconductor. However, it is not a conventional superconductor, rather it is an unconventional high temperature superconductor–meaning that its behavior cannot be explained with the conventional theories. Also, the superconducting behavior of the PdD_x lattice changes with the value of x.
- The deuterium in the PdD_x lattice is ionized deuterium. In other words, the electrons associated with the deuterons are in the conduction band.
- Pd does not follow the normal order for the filling of its electron shells. Rather, it fills the higher-level electron d shell before it fills the lower level electron s shell–specifically the s-electrons fill the d-band.
- One property of palladium hydride is its magnetic susceptibility. The susceptibility of PdD_x varies largely when changing the concentration of deuterium.
- Another metallic property of Pd is the electronic specific heat coefficient γ, which depends on the electronic density of states. For pure Pd, the heat coefficient is 9.5 mJ/(mol·K^2). When D is added to the Pd, the electronic heat coefficient drops. For the range of $\times = 0.83$ to $\times = 0.88$, γ is observed to be six times smaller than in the case of only Pd. This region is the superconducting region.

There are many other interesting behaviors and observations related to superconductors and electron stopping power. One of which is the defect production in PdD_x, due to excited ions and various energies. There are two contributions to the process of defect production in a metal lattice: Elastic displacement and electron excitation. Nuclear stopping power is related to elastic displacement, and electronic stopping power is related to electronic excitation. It appears that for superconducting materials, the defect production corresponds to the elastic displacement, rather than to the electronic excitation. Here is a quote from reference [33] regarding this behavior for superconductor of $EuBa_2Cu_3O_y$:

> "The slope of c-axis lattice parameter versus fluence, which corresponds to the defect production rate, is separated into two contributions; the effect via elastic displacement and the effect via electronic excitation. The contribution due to the effect via elastic displacement exhibits a linear increase versus the nuclear stopping power S_n."

Thus, from these experimental results, ions going through a superconductor are stopped by elastic collisions with nuclei, rather than by electron stopping. In other words, what dominates the defect production in this superconductor is the elastic collisions related to the nuclear stopping power, rather than the electron stopping power. Again quoting from reference [33]:

> "As can be seen in the figure, $(\Delta c/c_0)/\Phi$ for low energy ion irradiation is a linear function of S_n, ie, $(\Delta c/c_0)/\Phi = aS_n$, where $a = 3 \times 10^{16}$ mg/MeV. This means that the defect production rate is proportional to the energy transferred from the ion to the sample through elastic collisions....Therefore, we can conclude that elastic displacement is the dominant process of defect production for low energy ($\leq$ 2 MeV) ion irradiation."

In other words, for ion irradiation below 2 MeV, the creation of defects is due to the elastic collisions of the ions with the nuclei in the lattice. In superconductors, the process of electron stopping, under these conditions of ion energy below 2 MeV, is a negligible process.

In further studies, it is shown experimentally from Ishikawa et al. [34], that the defects due to ionization of a superconductor is strongly dependent on the nuclear stopping power. Also, the critical temperature T_c is strongly related only to S_n, rather than S_e. Quoting from the paper:

> "The defect production rate, which is obtained from the initial slope of the resistance–fluence curve, is almost proportional to the nuclear stopping power, S_n. The T_c depression due to irradiation is also nearly proportional to S_n. These results indicate that the defect production process is dominated by elastic displacement..."

Thus, experimental data implies that the effects of electron stopping on energetic ions inside of the lattice for a superconductor are strong mitigated. Unfortunately, no data has been taken about the ionic damage in the superconductor of PdD_x. However, if PdD_x is similar to these other superconducting materials, for which such data has been collected, these data do suggest that the dominant cause of crystal damage is due to nuclear stopping power, rather than by electronic excitation.

The reason for this can be better understood by examining the curves for stopping power, as in Figure 3 and Figure 4. If the curve of the electronic stopping power within the superconducting material of PdD_x is shifted to a higher energy due to the higher mobility of the electrons, then the energetic ions can travel further in the lattice. In other words, the nuclear stopping becomes the predominant slowing mechanism for low energy ($\leq$2 MeV) ions. Fortunately, it is this energy region, ion energies less than 2 MeV, that is of interest to LENR. If electron stopping power curves do indeed shift to higher energies for superconductors, as experimental data implies, then LENR reactions can take place within the palladium core. It is quite reasonable to assume that the superconducting material of PdD_x has some unusual and unexplained electronic behaviors, one of which would be that the electronic behavior of PdD_x is similar to other superconducting materials with regards to electron stopping power. With this assumption, LENR can then be explained by conventional nuclear explanations.

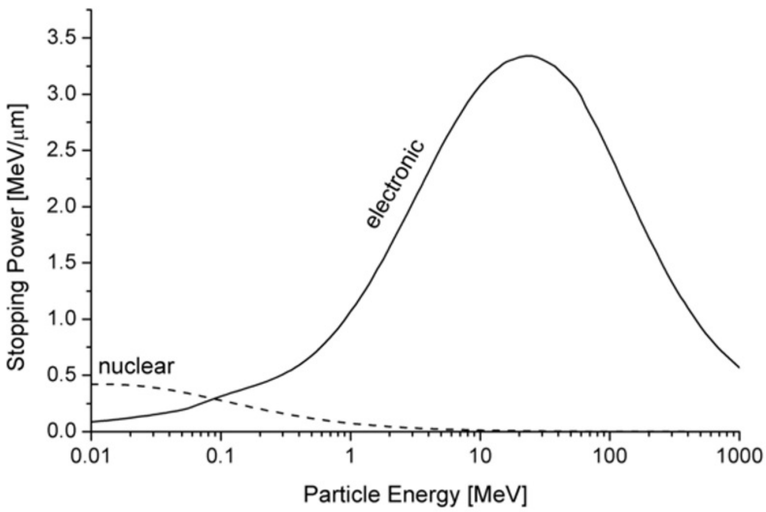

Figure 3. Plots of the stopping power for electron stopping and nuclear stopping shown as a generic diagram, illustrating the relative placement of the two effects with respect to each other, versus energy.

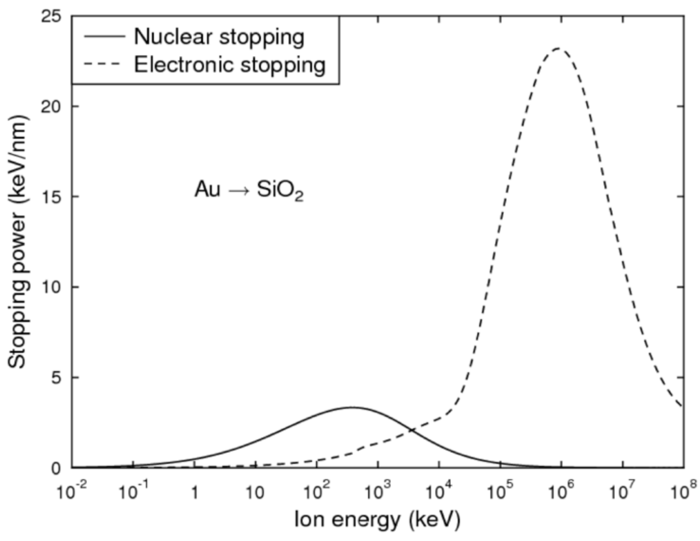

Figure 4. Plots of the stopping power for electron stopping and nuclear stopping for gold onto silicon-dioxide, illustrating the relative placement of the two effects with respect to each other, versus energy.

2.2.8. *The Effects of the Lattice on Reaction Rates*

As discussed above, the assistance of the lattice in the nuclear reaction rates is critical. Consider, for example, heavy water, wherein there is no lattice structure. Because of this lack of structure, even though there is a high concentration of deuterium, a nuclear reaction cannot take place. Heavy water has 6.68 $\times$ 10^{22} ions per cm^3, which is comparable to the density of fuel within the palladium lattice. However, nuclear reactions of ^{2}D+^{2}D do not occur in heavy water, and certainly a ^{2}D$-$ to ^{2}D chain reaction does not occur in heavy water. The reason the reaction does not take place in heavy water is due to electron stopping and the resulting braking action that the electrons impose upon the ions. In the PdD_x lattice, for high values of x, this braking action does not occur in a lattice—due to the phenomena of superconductivity, channeling, convey electrons, and electron shielding—along with the phonons and coherent movements that enable such phenomena.

While these lattice phenomena are indeed a reasonable explanation, there are no quantifiable measurements of this effect. One can only estimate that the phenomena of increased electron mobility, electron channeling, convey electrons, and electron shielding improve the ability of projectile ions to move through the lattice a reasonable distance, without incurring and excessive energy loss due to electron stopping. A significant increase in the distance an ion can traverse through a lattice—as a result of these phenomena—will correspondingly improve the reaction rate. In other words, all of these lattice properties of the palladium lattice—the complexities of the electric field within the lattice, the electron screening of the lattice, the convey electrons, channeling, etc.—can be incorporated into an effective maximum impact parameter for Coulomb elastic scattering. In this paper, the estimate of the improved reaction rate is able to be embodied in the one parameter of b_{max}. The effective maximum impact parameter, $b_{max\_effective}$, is estimated to be 3.93 $\times$ 10^{-7} m. This, then, is the one deviation from a conventional explanation of nuclear fusion—specifically, that the lattice is able to improve the reaction rate, due to the behavior of the electrons within the lattice.

2.3. Calculate the Scattering Rate of Energetic Protons with 2D

We have all the required equations needed to make the scattering calculations for the charged particles, for the example LENR reactor. We start with the child product of the proton.

For this example calculation, it is assumed that the density of the ^{2}D within the core Pd lattice, is that of a lattice that is loaded to 95%. As calculated previously, this gives the density as 5.387 $\times$ 10^{22} atoms/cm^3.

Upon its release from the first primary1 reaction, the initial kinetic energy of the proton is 3.03 MeV, with an initial velocity of 2.42 $\times$ 10^9 cm/sec. For our example, we assumed there was one watt of power being generated by the two primary reactions. The two primary reactions occur at equal probability. Thus, the primary1 reaction of ^{2}D+^{2}D —> ^{3}T+p occurs at 8.55 $\times$ 10^{11} times per second, releasing 8.55 $\times$ 10^{11} protons per second, each with an energy of 3.03 MeV. (The kinetic energy of the projectile causing the previous ^{2}D to ^{2}D reaction must also be also included, and this averages out to give an initial energy for the proton of 3.33 MeV.)

The summations are done from Θ_{CM_min} to Θ_{CM_max}. Using Eq. (30) for an energy of 3.33 MeV and with m_p = 1 and m_t = 2, it is found that the center-of-mass deflection angle $\Theta_{CM\_success}$ must be at least 15° for a successful scattering event. Using Eq. (24) and numerical integration, the expectation value of the projectile energy for all scatters is found to be 3.299999990 MeV, when the initial projectile energy is 3.33 MeV. (This is seen in Table 4, in the first row of Column E.) This value of the projectile energy needs to be re-calculated for all energies as the projectile slows down.

Using Eq. (11), the fractional energy loss per collision at the energy of 3.33 MeV is 3.139 $\times$ 10^{-10}. (Column I.) Using Eq. (34), the average number of times the proton scatters, N_{ave}, is calculated to be 2.88 $\times$ 10^7. (Column J.) For the successful scattering events only, the expectation value of the target energy is 0.2036 MeV. (Column M.) Column N is used to calculate the weighted average. These calculations are for a proton at 3.33 MeV, shown in row 1 of Table 4. These calculations are repeated for every energy from 3.33 MeV to 0.1 MeV, in steps of 0.1 MeV, as shown in Table 4.

Table 4. For the proton projectiles of primary1 reaction, this is the number of energetic ^{2}D targets and their expectation energy, $E_{tf\_success}$, for successful scattering events. E_{tf} is the final energy of the target, for the successfully scattered targets.

A	B	C	D	E	F	G	H	I	J	K	L	M	N
E_{pi} (Initial energy of the projectile) in MeV	For the energy in each row, Θ_{cM_min} in degrees, rounded.	The numerical integration of $P(\Theta)$, summed from Θ_{CM_min} to Θ_{CM_2xx}.	The numerical integration of $P(\Theta)*(E_{pf}/E_{pi})$, summed from Θ_{aM_min} to Θ_{CM_max}.	Expectation energy $E_{pf}(\Theta)$ in MeV, from Θ_{min} to Θ_{max}	COM angle, where successful scattering starts. Rounded.	The numerical integration of $P(0)$, summed from $\Theta_{CM\_success}$ to Θ_{CM_max}.	Fraction of successful scatters after one collsion.	Fractional energy loss per collision	Average number of times, N, the projectile collides before falling to the next lower energy level.	Expectation value of E_{pf} for the successful scatterers only, in MeV.	Number of successful scatters.	Expectation energy E_{tf} for the ^{2}D targets, for successful scatters, in MeV.	Expectation energy E_{tf} for only the successful scatters times the number of successful scatters
3.33	9.5E-08	3.628E+08	3.628E+08	3.3299999990	15.0	1.006976	2.775E-09	3.139E-10	2.88E+07	3.1264	6.84E+10	0.2036	1.39E+10
3.3	0.0000001	3.628E+08	3.628E+08	3.2999999990	15.0	1.006976	2.775E-09	3.139E-10	9.80E+07	3.0983	2.33E+11	0.2017	4.69E+10
3.2	0.0000001	3.628E+08	3.628E+08	3.1999999990	15.0	1.006976	2.775E-09	3.139E-10	1.01E+08	3.0044	2.40E+11	0.1956	4.69E+10
3.1	0.0000001	3.091E+08	3.091E+08	3.0999999989	16.0	0.883634	2.859E-09	3.685E-10	8.90E+07	2.8906	2.17E+11	0.2094	4.55E+10
3	0.00000011	3.091E+08	3.091E+08	2.9999999989	16.0	0.883634	2.859E-09	3.685E-10	9.20E+07	2.7974	2.25E+11	0.2026	4.56E+10
2.9	0.00000011	3.091E+08	3.091E+08	2.8999999989	16.0	0.883634	2.859E-09	3.685E-10	9.52E+07	1.2227	2.33E+11	1.6773	3.90E+11
2.8	0.00000011	2.693E+08	2.693E+08	2.7999999988	16.0	0.883634	3.281E-09	4.229E-10	8.60E+07	2.6109	2.41E+11	0.1891	4.56E+10
2.7	0.00000012	2.693E+08	2.693E+08	2.6999999989	17.0	0.781411	2.902E-09	4.229E-10	8.92E+07	2.4999	2.21E+11	0.2001	4.43E+10
2.6	0.00000012	2.391E+08	2.391E+08	2.5999999988	17.0	0.781411	3.269E-09	4.765E-10	8.23E+07	2.4073	2.30E+11	0.1927	4.43E+10
2.5	0.0000001	2.391E+08	2.391E+08	2.4999999988	17.0	0.781411	3.269E-09	4.765E-10	8.57E+07	2.3147	2.39E+11	0.1853	4.44E+10
2.4	0.0000001	2.391E+08	2.391E+08	2.3999999989	18.0	0.695749	2.910E-09	4.765E-10	8.93E+07	2.2059	2.22E+11	0.1941	4.31E+10
2.3	0.0000001	2.155E+08	2.155E+08	2.2999999988	18.0	0.695749	3.228E-09	5.285E-10	8.41E+07	2.1140	2.32E+11	0.1860	4.32E+10
2.2	0.00000014	1.968E+08	1.968E+08	2.1999999987	18.0	0.695749	3.535E-09	5.787E-10	8.04E+07	2.0221	2.43E+11	0.1779	4.32E+10
2.1	0.00000015	1.968E+08	1.968E+08	2.0999999988	19.0	0.623253	3.166E-09	5.787E-10	8.43E+07	1.9157	2.28E+11	0.1843	4.21E+10
2	0.00000016	1.818E+08	1.818E+08	1.9999999987	19.0	0.623253	3.429E-09	6.267E-10	8.19E+07	1.8245	2.40E+11	0.1755	4.21E+10
1.9	0.00000017	1.694E+08	1.694E+08	1.8999999987	20.0	0.561358	3.313E-09	6.723E-10	8.04E+07	1.7200	2.28E+11	0.1800	4.10E+10
1.8	0.00000018	1.592E+08	1.592E+08	1.7999999987	21.0	0.508093	3.191E-09	7.155E-10	7.99E+07	1.6166	2.18E+11	0.1834	4.00E+10
1.7	0.00000019	1.506E+08	1.506E+08	1.6999999987	21.0	0.508093	3.373E-09	7.561E-10	8.02E+07	1.5268	2.31E+11	0.1732	4.00E+10
1.6	0.0000002	1.434E+08	1.434E+08	1.5999999987	22.0	0.461926	3.221E-09	7.944E-10	8.12E+07	1.4254	2.24E+11	0.1746	3.91E+10
1.5	0.00000021	1.372E+08	1.372E+08	1.4999999988	22.0	0.461926	3.367E-09	8.302E-10	8.31E+07	1.3364	2.39E+11	0.1636	3.91E+10
1.4	0.00000023	1.319E+08	1.319E+08	1.3999999988	23.0	0.421650	3.197E-09	8.637E-10	8.58E+07	1.2370	2.35E+11	0.1630	3.82E+10
1.3	0.00000024	1.232E+08	1.232E+08	1.2999999988	24.0	0.386303	3.135E-09	9.243E-10	8.66E+07	1.1390	2.32E+11	0.1610	3.74E+10
1.2	0.00000026	1.166E+08	1.166E+08	1.1999999988	25.0	0.355113	3.046E-09	9.771E-10	8.91E+07	1.0424	2.32E+11	0.1576	3.66E+10
1.1	0.00000029	1.113E+08	1.113E+08	1.0999999989	26.0	0.327453	2.941E-09	1.023E-09	9.32E+07	0.9472	2.34E+11	0.1528	3.58E+10
1	0.0000003	1.054E+08	1.054E+08	0.9999999989	28.0	0.260952	2.477E-09	1.081E-09	9.75E+07	0.9099	2.06E+11	0.0901	1.86E+10
0.9	0.0000004	9.561E+07	9.561E+07	0.8999999989	29.0	0.226935	2.374E-09	1.191E-09	9.89E+07	0.8672	2.01E+11	0.0328	6.58E+09
0.8	0.0000004	7.408E+07	7.408E+07	0.7999999988	31.0	0.198915	2.685E-09	1.538E-09	8.68E+07	0.7505	1.99E+11	0.0495	9.87E+09
0.7	0.0000005	6.974E+07	6.974E+07	0.6999999989	33.0	0.198915	2.852E-09	1.633E-09	9.44E+07	0.5645	2.30E+11	0.1355	3.12E+10
0.6	0.0000005	6.651E+07	6.651E+07	0.5999999990	36.0	0.165320	2.486E-09	1.713E-09	1.06E+08	0.4695	2.26E+11	0.1305	2.95E+10
0.5	0.0000010	5.963E+07	5.963E+07	0.4999999990	39.0	0.139181	2.334E-09	1.910E-09	1.17E+08	0.3792	2.33E+11	0.1208	2.82E+10
0.4	0.0000010	5.963E+07	5.963E+07	0.3999999992	44.0	0.106920	0.000000	1.910E-09	1.51E+08	0.2873	2.31E+11	0.1127	2.60E+10
0.3	0.0000010	5.963E+07	5.963E+07	0.2999999994	52.0	0.073369	0.000000	1.910E-09	2.12E+08	0.1964	2.23E+11	0.1036	2.31E+10
0.2	0.0000020	5.963E+07	5.963E+07	0.1999999996	64.0	0.044699	0.000000	1.91E-09	3.63E+08	0.1125	2.33E+11	0.0875	2.03E+10
0.1	0.000003	2.608E+07	2.608E+07	0.0999999996	98.0	0.013189	5.056E-10	4.367E-09	2.41E+07	0.0341	1.04E+10	6.59E-02	6.87E+08
0.09	0.000004	2.608E+07	2.608E+07	0.0899999996	105.0	0.010276	3.94E-10	4.367E-09	2.70E+07	0.0274	9.09E+09	6.26E-02	5.69E+08
0.08	0.000004	1.494E+07	1.494E+07	0.0799999994	115.0	0.007084	4.74E-10	7.622E-09	1.75E+07	0.0205	7.10E+09	5.95E-02	4.22E+08
0.07	0.000005	1.494E+07	1.494E+07	0.0699999995	120.0	0.005818	3.893E-10	7.622E-09	2.02E+07	0.0165	6.73E+09	5.35E-02	3.60E+08
0.06	0.000005	9.787E+06	9.787E+06	0.0599999993	120.0	0.005818	5.944E-10	1.164E-08					
								Number of successful scattered deuteron targets =			7.4027E +12		1.52E+12
								Average energy of the successful scattered deuteron targets =				0.2059	MeV

Column A shows the initial energy of the proton projectiles, in the lab reference frame. Column B shows the Θ_{CM_min} for each initial projectile energy, as calculated with Eq. (29) and then rounded. Column C is the numerical integration of the probability, from Θ_{CM_min} to Θ_{CM_max}. For the initial projectile energy in column A, this will be the denominator of Eq. (24). Column D is the numerical integration of the probability times the projectile energy, for the angles from Θ_{CM_min} to Θ_{CM_max}. This will be the numerator of Eq. (24), for the initial projectile energy in shown in column A. Column E is the expectation value of the final projectile energy after one collision for the initial projectile energy shown in column A.

Column F is the minimum center-of-mass angle for a successful scatter, $\Theta_{CM\_success}$, as calculated with Eq. (30), and rounded to the nearest degree. Column G is the numerical integration of the probability, from $\Theta_{CM\_success}$ to Θ_{CM_max}. This is the numerator for Eq. (27). Column H is the fraction of successful scattering events, after one scatter cycle. As can be seen, this is a small fraction. Column I is the fractional energy loss after one average scattering event; this uses the expectation energy in column E to determine the average fraction of energy that is lost by the projectile and transferred to the target. Column J is the average number of times, N, that the projectile scatters before losing energy, and going down to the next lower energy level. This is based on the value in column I, and uses Eq. (32).

Shown in column K is the expectation value for the successfully scattered projectiles, in MeV, after one scatter. This is the energy retained by the projectile. Shown in column L is the average number of times that the projectile scatters before losing energy, N, multiplied by the fraction of successful scattering events, multiplied by the initial number of projectiles. This number in column L is the number of successful scattering events as a result of these energetic protons, for just this one energy only. This column is summed at the bottom of Table 4, below column L, for all energies going from 3.33 MeV to 0.06 MeV. This summation value below column L is the total number of successful scatters attributed to the proton projectiles emitted in the primary1 reaction. As can be seen, there are 7.4027×10^{12} energetic ^{2}D, as a result of the energetic protons emitted in primary1 reaction, with an average energy of 0.2059 MeV. This number of energetic deuterons occurs each second, for the conditions outlined in this example. These values will be used in Section 5.

The energetic protons of Primary1 reaction could escape the Pd core, and if this happens, this would be a loss–not only of the particles, but also of the kinetic energy they contain. In this calculation, it is estimated that 0.1% of the energetic protons will escape the palladium core for each energy range, a generous amount.

In summary, an energetic proton collides with ^{2}D targets, transferring some of its kinetic energy as a result. The energetic proton projectiles scatter off the Pd and the ^{2}D. (When they scatter off the Pd, they lose very little of their energy, due to the large mass difference.) The protons give up only a small fraction of their energy, on average, with each collision. As the average speed of the average proton loses its energy, and goes to a lower energy, the deflection angle for a successful scatter is adjusted in the calculations to make sure that the final energy of the target, E_{tf}, is at least 0.1 MeV. The minimum deflection angle Θ_{CM_min} is also affected, since it is dependent on the projectile's velocity. Thus, the integration limits change as the energy decreases, affecting the probability function P(Θ) and the expectation value of both the projectile and target energies. Through numerical integration, these functions have been determined for one energy range. This process is then repeated, as the initial projectile energy steps down, going down until the projectile energy falls below 0.1 MeV. The total expectation energy of the projectiles has been found for this one projectile type—the energetic protons from Primary 1 reaction. From this, the total number and expectation energy of the successfully scattered ^{2}D targets is found. This entire process is repeated for the child product of ^{3}T.

2.4. 3T Scattering with 2D

Upon its release from the primary1 reaction, the triton has a kinetic energy of 1.01 MeV. Similar to the proton just considered, we want to know how many of these tritium projectiles successfully scatter with a ^{2}D atom, transferring a sufficient amount kinetic energy to the ^{2}D so that the ^{2}D might then react. To do this, we use the same Coulomb scattering techniques described above, but with a projectile of mass number A $= 3$ and the very first initial energy of 1.11 MeV. The results are shown in Table 5.

The expectation value of the projectile energy for all scatters is 1.109999999 MeV (first row of column E.) The fraction of successful scattering events yields the fraction of $= 2.271 \times 10^{-9}$ for the ^{3}T projectile onto a ^{2}D target (first row of column H.) The fractional energy loss per collision at this energy is 8.814×10^{-10}. (first row of column I.) The average number of times the proton scatters, N, is 1.0267×10^7 (first row of column J.) For the successful scattering events, the expectation value of the target energy is 0.1575 MeV (first row of column M.) These calculations are repeated, for every energy from 1.11 MeV to 0.1 MeV. (Column N is used to calculate the weighted average.)

Columns A through J are the same as in Table 4, but for a triton projectile instead of a proton. Column L is summed at the bottom of Table 5 for all energies going from 1.11 MeV to 0.01 MeV. This summation is the total number of successful scatters attributed to the triton projectiles that were emitted in the primary1 reaction. There are 2.016×10^{12} energetic ^{2}D per second with an average energy of 0.1311 MeV, as a result of the collisions with the excited tritons from primary1 reaction. These values are used in Section 5.

2.5. ^{3}He Scattering with 2D

The ^{3}He has a kinetic energy of 0.8175 MeV upon its emission from the primary2 reaction. Adding in the average kinetic energy of the projectile inciting that previous reaction, as is correct to do, the average energy is of the newly-released ^{3}He is 0.915 MeV.

Since this calculation is similar to the other projectile ions just considered, the details will not be described. We use the mass number A $= 3$ and Z $= 2$ for the projectile, with the initial first energy of 0.915 MeV. The results of the calculation are seen in Table 6.

Columns A through N are the same as in Tables 4 and 5, but using as the ^{3}He projectile. Column L is summed at the bottom of the Table 6 for all energies, from 0.915 MeV to 0.1 MeV. This summation is the total number of successful scatters attributed to the ^{3}He projectiles emitted in the primary2 reaction. As can be seen, there are 1.698×10^{12} energetic ^{2}D energized as a result of the energetic ^{3}He projectiles, for the conditions outlined in this example. The average energy of the ^{2}D targets resulting from these protons as 0.1254 MeV. These values are used later in Section 5.

2.6. Neutron Scattering with 2D

Neutrons have no charge, therefore the calculations for neutron scattering are different than the calculations used for charged particles. The data for the neutron scattering parameters for the various nuclides is reproduced here in Table 7 [35]:

Column A and B of Table 7 show the nuclide and its atomic weight. The logarithmic energy decrement, typically represented by the Greek letter ξ (ksi), is shown in column C for that nuclide. The average number of scattering events, N, to bring the neutron energy down to ambient temperature is shown in column D and E. The average fraction of retained energy after one scattering event is shown in Column F.

On average, the fraction of retained energy for a neutron after one scatter with a deuteron is 0.4842, or 48.42%. Note that neutron scattering is independent of the scattering deflection angle, and that the logarithmic energy decrement ξ is independent of the initial energy.

As with the charged-particle scattering, our goal is to find the number and average energy of successfully scattered ^{2}D targets that scatter from these neutrons. To do this, we need the probability, $P_{\text{n-to-D}}$, that a neutron will scatter with a ^{2}D for a given energy. This probability is the product of three terms: the scattering cross section σ_{scatter} at that energy, the distance the neutron travels, and the number density ρ_{target} of the target. This is shown in Eq. (36).

$$P_{n-to-D} = (\sigma_{\text{scatter}})\,(\text{distance})\,(\rho_{\text{target}}) \tag{36}$$

Table 5. For the triton projectiles of primary1 reaction, this is the number of energetic ^{2}D targets and their target expectation energy, $E_{tf\_success}$ for successful scattering events.

A	B	C	D	E	F	G	H	I	J	K	L	M	N
Initial projectile energy, E_{pi}, in MeV	For the energy in each row, $\Theta_{\text{CM\_min}}$ in degrees, rounded.	The numerical integration of $P(\Theta)$, summed from $\Theta_{\text{CM\_min}}$ to $\Theta_{\text{CM\_max}}$.	The numerical integration of $P(\Theta) * (E_{\text{pf}}/E_{\text{pi}})$, summed from $\theta_{\text{CM\_2 in}}$ to $\Theta_{\text{CM\_max}}$.	Expectation energy $E_{\text{pf}}(\Theta)$ in MeV, from $\Theta_{\min}$ to $\Theta_{\max}$.	COM angle, where successful scattering starts. Rounded.	The numerical integration of $P(\Theta)$, summed from $\Theta_{\text{CM\_success}}$ to $\Theta_{\text{CM\_max}}$.	Fraction of successful scatters after one collsion.	Fractional energy loss per collision	Average number of times, N, the projectile collides before falling to the next lower energy level.	Expectation value of E_{pf} for the successful scatterers only, in MeV.	Number of successful scatters.	Expectation value of the target final energy, E_{tf}, for the ^{2}D targets, for only the successful scatters, in MeV.	Expectation energy E_{tf} for only the successful scatters times the number of successful scatters
1.11	0.0000005	1.5636E+08	1.5636E+08	1.109999999	10	0.355113	2.271E-09	8.814E-10	1.0267E+07	0.9525	1.994E+10	0.1575	3.14E+09
1.1	0.0000005	1.0479E+08	1.0479E+08	1.099999999	10.1	0.355113	3.389E-09	1.315E-09	7.2469E+07	0.9440	2.100E+11	0.1560	3.28E+10
1	0.0000005	1.0479E+08	1.0479E+08	0.999999999	10.6	0.302810	2.890E-09	1.315E-09	8.0111E+07	0.8417	1.979E+11	0.1583	3.13E+10
0.9	0.0000006	7.6781E+07	7.6781E+07	0.899999998	11.1	0.280760	3.657E-09	1.795E-09	6.5618E+07	0.7500	2.051E+11	0.1500	3.08E + 10
0.8	0.0000007	7.6781E+07	7.6781E+07	0.799999998	11.8	0.243093	3.166E-09	1.795E-09	7.4391E+07	0.6532	2.014E+11	0.1468	2.96E+10
0.7	0.0000008	5.9891E+07	5.9891E+07	0.699999998	12.6	0.212268	3.544E-09	2.301E-09	6.6987E+07	0.5597	2.030E+11	0.1403	2.85E+10
0.6	0.0000009	4.8929E+07	4.8929E+07	0.599999998	13.7	0.175563	3.588E-09	2.817E-09	6.4727E+07	0.4643	1.986E+11	0.1357	2.70E+10
0.5	0.0000011	3.6037E+07	3.6037E+07	0.499999998	15	0.147209	4.085E-09	3.824E-09	5.8347E+07	0.3739	2.038E+11	0.1261	2.57E+10
0.4	0.0000013	2.9034E+07	2.9034E+07	0.399999998	16.8	0.118447	4.080E-09	4.747E-09	6.0605E+07	0.2852	2.114E+11	0.1148	2.43E+10
0.3	0.0000018	2.1049E+07	2.1049E+07	0.299999998	19.4	0.084037	3.992E-09	6.548E-09	5.1777E+06	0.1958	1.767E+10	0.1042	1.84E+09
0.29	0.0000018	2.1049E+07	2.1049E+07	0.289999998	19.8	0.080266	3.813E-09	6.548E-09	5.3594E+06	0.1868	1.747E+10	0.1032	1.80E+09
0.28	0.0000019	2.0193E+07	2.0193E+07	0.279999998	20.1	0.076716	3.799E-09	6.8253E-09	5328327.299	0.1779	1.731E+10	0.1021	1.77E+09
0.27	0.0000019	2.0193E+07	2.0193E+07	0.269999998	20.5	0.073369	3.633E-09	6.8253E-09	5529443.21	0.1693	1.718E+10	0.1007	1.73E+09
0.26	0.000002	1.9468E+07	1.9468E+07	0.259999998	20.9	0.070211	3.607E-09	7.0795E-09	5540022.611	0.1608	1.708E+10	0.0992	1.69E+09
0.25	0.0000021	1.8849E+07	1.8849E+07	0.249999998	21.3	0.067227	3.567E-09	7.312E-09	5582867.024	0.1525	1.703E+10	0.0975	1.66E+09
0.24	0.000002	1.8849E+07	1.8849E+07	0.239999998	21.8	0.061735	3.275E-09	7.312E-09	5820506.095	0.1424	1.630E+10	0.0976	1.59E+09
0.23	0.000002	1.8849E+07	1.8849E+07	0.229999998	22.3	0.059204	3.141E-09	7.312E-09	6079278.642	0.1345	1.633E+10	0.0955	1.56E+09
0.22	0.000002	1.8849E+07	1.8849E+07	0.219999998	22.8	0.056803	3.014E-09	7.312E-09	6362135.518	0.1269	1.639E+10	0.0931	1.53E+09
0.21	0.000003	1.8849E+07	1.8849E+07	0.209999998	23.4	0.052360	2.778E-09	7.312E-09	6672603.871	0.1176	1.585E+10	0.0924	1.46E+09
0.2	0.000003	1.8849E+07	1.8849E+07	0.199999999	24	0.048343	2.565E-09	7.312E-09	7014935.09	0.1088	1.538E+10	0.0912	1.40E+09
0.19	0.000003	1.5665E+07	1.5665E+07	0.189999998	24.6	0.046477	2.967E-09	8.798E-09	6145572.945	0.1018	1.559E+10	0.0882	1.37E+09
0.18	0.000003	1.5665E+07	1.5665E+07	0.179999998	25.3	0.043003	2.745E-09	8.798E-09	6496934.456	0.0936	1.525E+10	0.0864	1.32E+09
0.17	0.000003	1.5665E+07	1.5665+07	0.169999999	26.1	0.039839	2.543 E-09	8.798E-09	6890922.401	0.0857	1.498E+10	0.0843	1.26E+09
0.16	0.000003	1.5665E+07	1.5665+07	0.159999999	26.9	0.035598	2.272E-09	8.798E-09	7335797.459	0.0769	1.425E+10	0.0831	1.18E+09
0.15	0.000004	1.5665E+07	1.5665E+07	0.149999999	27.9	0.033064	2.111E-09	8.798E-09	7842103.017	0.0698	1.415E+10	0.0802	1.14E+09
0.14	0.000004	1.4551E+07	1.4551E+07	0.139999999	28.9	0.029643	2.037E-09	9.471E-09	7824456.044	0.0620	1.363E+10	0.0780	1.06E+09
0.13	0.000004	1.4551E+07	1.4551E+07	0.129999999	30	0.029643	2.037E-09	9.471E-09	8451056.438	0.0576	1.472E+10	0.0724	1.07E+09
0.12	0.000004	1.4551E+07	1.4551E+07	0.119999999	31.3	0.025684	1.765E-09	9.471E-09	9186821.374	0.0496	1.386E+10	0.0704	9.76E+08
0.11	0.000005	9.3948E+06	9.3948E+06	0.109999998	32.8	0.023097	2.458E-09	1.467E-08	6496958.495	0.0431	1.366E+10	0.0669	9.13E+08
0.1	0.000005	9.3948E+06	9.3948E+06	0.099999999	34.5	0.019381	2.063E-09	1.467E-08	7182054.465	0.0358	1.267E+10	0.0642	8.13E+08
0.09	0.000006	6.5936E+06	6.5936 E +06	0.089999998	36.4	0.015717	2.384E-09	2.090E-08	5634984.331	0.0287	1.148E+10	0.0613	7.04E+08
0.08	0.000007	6.5936E+06	6.5936E+06	0.079999998	38.6	0.012731	1.931E-09	2.090E-08	6388418.34	0.0226	1.055E+10	0.0574	6.05E+08
0.07	0.000008	4.9046E + 06	4.9046E+06	0.069999998	40.8	0.009213	1.878E-09	2.810E-08	5485775.024	0.0163	8.810E+09	0.0537	4.74E+08
0.06	0.000009	3.8084E+06	3.8084E+06	0.059999998	41.8	0.006056	1.590E-09	3.619E-08	5038118.252	0.0107	6.850E+09	0.0493	3.38E+08
0.05	0.000011	2.5193E+06	2.5193E+06	0.049999997		0.019381	7.693E-09	5.471E-08	4078908.047				
0.04	0.000013	1.8190E+06	1.8190E+06	0.039999997		0.019381	1.065E-08	7.577E-08	3796885.631				
0.03	0.000018	1.0205E+06	1.0205E+06	0.029999996		0.019381	1.899E-08	1.351E-07	3002161.469				
0.02	0.000026	5.9413E+05	5.9413E+05	0.019999995		0.019381	3.262E-08	2.320E-07	2988081.679				
0.01	0.000053	3.1911E+05	3.1911E+05	0.009999996		0.019381	6.073E-08	4.319E-07	5331413.069				
0.001		0	0					Number of successful scattered deuteron targets =			2.016E+12		2.64E+11
									Average energy of the successful scattered deuteron targets =			0.1311	MeV

Table 6. For the ^{3}He projectiles of primary2 reaction, this is the number of energetic ^{2}D targets and their target expectation energy, $E_{tf\_success}$ for successful scattering events.

A	B	C	D	E	F	G	H	I	J	K	L	M	N
E_{pi}, in MeV	For the energy in each row, $\Theta_{\mathrm{CM\_min}}$ in degrees, rounded.	The numerical integration of $P(\Theta)$, summed from $\Theta_{\mathrm{CM\_min}}$ to $\Theta_{\mathrm{CM\_max}}$.	The numerical integration of $P(\Theta) *$ $(E_{\mathrm{pf}}/E_{\mathrm{pi}})$, summed from $\Theta_{\mathrm{CM\_min}}$ to $\Theta_{\mathrm{CM\_max}}$.	Expectation energy Epf(Θ) in MeV, from Θmin to Θmax.	COM angle, where successful scattering starts. Rounded.	The numerical integration of $P(\Theta)$, summed from OCM_success to OCM_max.	Fraction of successful scatters after one collsion.	Fractional energy loss per collision	Average number of times, N, the projectile collides before falling to the next lower energy level.	Expectation value of Epf for the successful scatterers only, in MeV.	Number of successful scatters.	Expectation energy Etf for the 2D targets, for successful scatters, in MeV.	Expectation energy Etf for only the successful scatters times number of successful scatters
0.9150	0.0000011	3.2060E+07	3.2060E+07	0.914999996	28	0.280760	8.757E-09	4.2989E-09	3.84503E+06	0.762537	2.879E+10	0.1525	4.39E+09
0.9	0.0000012	3.2060E+07	3.2060E+07	0.899999996	28	0.280760	8.757E-09	4.2989E-09	2.73985E+07	0.750036	2.051E+11	0.1500	3.08E+10
0.8	0.0000013	2.9034E+07	2.9034E+07	0.799999996	30	0.243093	8.373E-09	4.7468E-09	2.81308E+07	0.653244	2.014E+11	0.1468	2.96E+10
0.7	0.0000015	2.4812E+07	2.4812E+07	0.699999996	32	0.212268	8.555E-09	5.5546E-09	2.77519E+07	0.559683	2.030E+11	0.1403	2.85E+10
0.6	0.0000018	2.1049E+07	2.1049E+07	0.599999996	35	0.175563	8.341E-09	6.5476E-09	2.78457E+07	0.464268	1.986E+11	0.1357	2.70E+10
0.5	0.0000021	1.8849E+07	1.8849E+07	0.499999996	38	0.147209	7.810E-09	7.3120E-09	3.05174E+07	0.373910	2.038E+11	0.1261	2.57E+10
0.4	0.0000026	1.6786E+07	1.6786E+07	0.399999997	42	0.118447	7.056E-09	8.2105E-09	3.50383E+07	0.285239	2.114E+11	0.1148	2.43E+10
0.3	0.000004	1.5665E+07	1.5665E+07	0.299999997	50	0.080266	5.124E-09	8.7978E-09	4.60874E+07	0.193221	2.019E+11	0.1068	2.16E+10
0.2	0.000005	9.3948E+06	9.3948E+06	0.199999997	62	0.048343	5.146E-09	1.4670E-08	4.72494E+07	0.108775	2.079E+11	0.0912	1.90E+10
0.1	0.000011	2.5193E+06	2.5193E+06	0.099999995	93	0.015717	6.239E-09	5.4707E-08	1.92592E+06	0.031898	1.027E+10	0.0681	7.00E+08
0.09	0.000012	2121512.88	2121512.741	0.089999994	100	0.012289	5.792E-09	6.4963E-08	1813065.554	0.024892	8.979E+09	0.0651	5.85E+08
0.08	0.000013	1818986.954	1818986.816	0.079999994	108	0.009213	5.0649E-09	7.5768E-08	1762374.073	0.018579	7.632E+09	0.0614	4.69E+08
0.07	0.000015	1396739.146	1396739.008	0.069999993	121	0.005587	3.9999E-09	9.8673E-08	1562233.297	0.011886	5.343E+09	0.0581	3.10E+08
0.06	0.000018	1020458.693	1020458.555	0.059999992	131	0.003625	3.5521E-09	1.3506E-07	1349952.787	0.007800	4.100E+09	0.0522	2.14E+08
0.05													
										Sum =	1.6982E+12		2.13E+11
											Average energy of the successful scattered deuteron targets =	0.1254	MeV

Table 7. A sample of the neutron scattering parameters for various nuclides.

A	B	C	D	E	F
nuclide	A, atomic weight	ξ, ksi, the logarithmic energy decrement	Average number of scattering events, N, to reach thermal energy from 2.4525 MeV	integer N	Average fraction of retained energy after one scatter
H-1	1	1.0000	20.1544	20	0.3679
D-2	2	0.7253	27.7858	27	0.4842
Li-6	6	0.2990	67.4023	67	0.7415
0-16	16	0.1199	168.0278	168	0.8870
Pd-106	106	0.0187	1074.910745	1074	0.9814

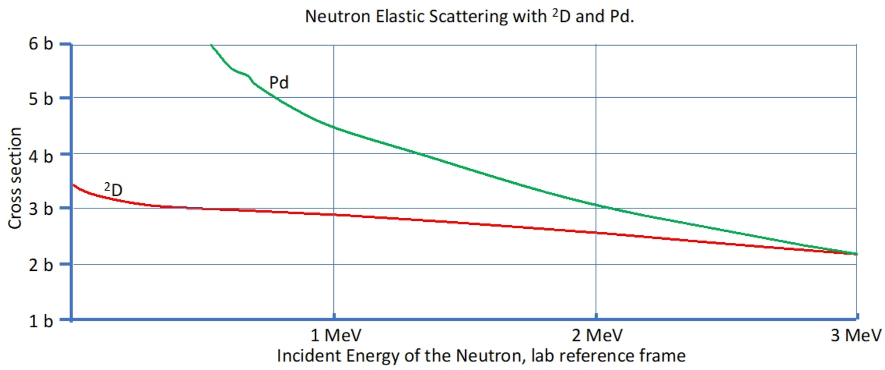

Figure 5. Linear plot of cross section vs. incident lab neutron energy for the elastic n-to-D and n-to-Pd scattering.

The cross section for the scattering event, $\sigma_{scatter}$, is found from the experimental data for neutrons scattering off deuterium and palladium [36], [37]. This is reproduced here in Figure 5.

For each initial incident energy of the neutron, the scattering cross section is obtained from these plots and used in the Eq. (36). A neutron emitted from primary2 reaction has 2.453 MeV of kinetic energy. As can be seen in in Figure 5, when a neutron scatters off deuterium, the curve is fairly flat over the energy range of interest, with a value ranging between 2.5 to 3.5 barns. At 2.453 MeV, this gives the scattering cross section as 2.37 barns $= 2.37 \times 10^{-24}$ cm^2 for deuterium. For palladium, at 2.453 MeV, the cross section is 2.7 barns.

For Eq. (36), the distance is how far the neutron traverses through the palladium within the core. For a 1 cm^3 core of Pd, with the shape as described for this example, the average total distance traveled through the palladium is calculated to be about 1.35 cm, and an equal distance going through the electrolyte between the layers of the core.

When travelling through the palladium core, the energetic neutron has the opportunity to scatter off of a palladium atom or off a deuteron. If a neutron does not scatter, and instead escapes the Pd core, then it may scatter in the electrolyte, and re-enter the palladium core. If it does not re-enter the palladium core, then the neutron and its kinetic energy are lost from the core. Alternatively, if the neutron does scatter within the core or if it re-enters the core, then it has another opportunity to scatter again, either with a palladium atom or a deuteron.

The rolled-up foil shape, used in this example, is optimum for confining the neutrons within the palladium core as much as possible. If a neutron escapes one part of the palladium core, it is very likely to re-enter another part of the

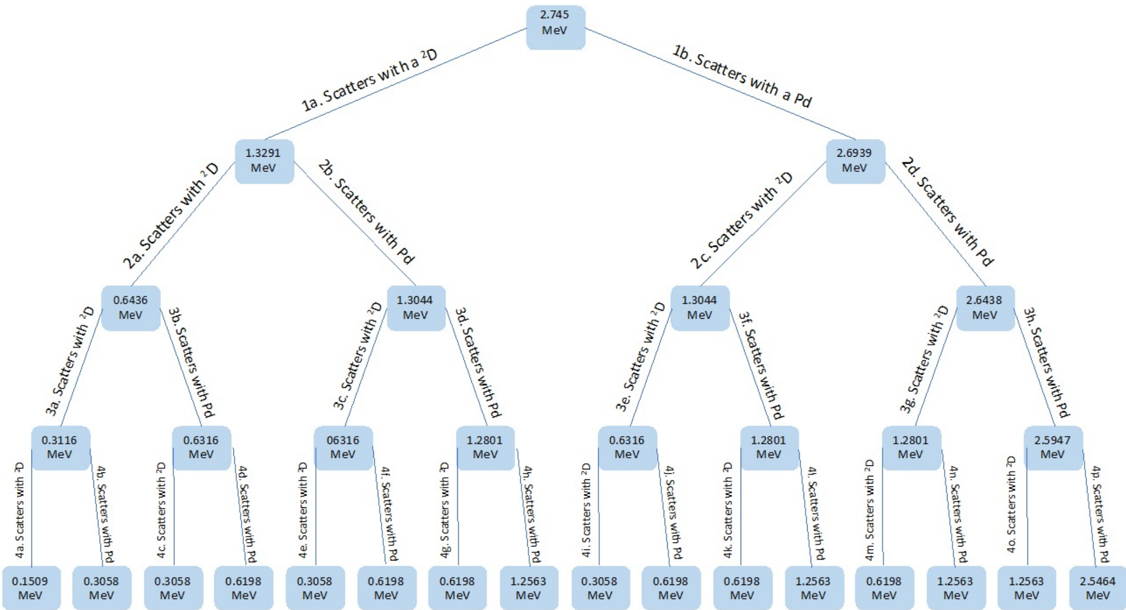

Figure 6. A diagram of neutron scattering and the resultant energies, for four scatters. There are 16 different possible paths for a neutron during those four scatters.

core. Other shapes that exhibit this same ability to confine the neutrons are a sponge-like interconnection of numerous tiny particles, several long rods bundled together, or numerous thin wires meshed together in a compacted ball. If a neutron escapes one part of the palladium core, it will be slowed down by the electrolyte and very likely reenter another part of the core. (Long rods bundled together is the core shape used by most fission reactors to contain the neutrons, thereby maintaining the chain reaction within the core.)

The many different possible scattering paths of a neutron scattering off the palladium or deuterons are illustrated in the Figure 6 below.

Each level in Figure 6 represents one of the four scattering events that could possibly take place when a neutron scatters. Each scatter event branches with two possibilities, one in which the neutron scatters with a ^{2}D, and one in which the neutron scatters with a Pd. Depending on the branch, the resulting energies are different. The neutron then goes on to scatter again with the next scattering event, again with two branching possibilities. This chart shows all of the possibilities for a neutron to scatter, resulting in the various final energies, shown at the lowest most level, after four scattering events. This information is also represented in Table 8

In Table 8, Column A is the scattering number, to identify the four scatter events in Figure 6. Column B is the energy of the neutron for this scatter. Column C is the velocity of the neutron before the scatter. Column D identifies the target, of which there are three possible targets: ^{2}D in the palladium core, ^{2}D in the electrolyte contained within the core, and the Pd of the core. All three of these possible targets will have a different effect on the neutron when it scatters, and all three of these possible targets have a different probability for scattering the neutron.

Column E shows the average kinetic energy of the neutron after the scatter. This kinetic energy is what goes onward to the next scattering event for the neutrons. This is color coded, for ease of understanding where this energy is transferred to the next subsequent scatter. Also, the number of neutrons still in the core is determined, shown in

Table 8. Neutron scattering with deuterium, electrolyte, and the palladium.

A	B	c	D	E	F	G	H	I	I	K	L	M	N
Scattering number and identifier	Neutron energy before collision in MeV	Neutron velocity before collision, in cm/sec	Target of the collision	Average Neutron Energy after collision with target, in MeV	Number of hot neutrons in the core	Scattering Cross section with target, in barns, at this incident energy.	Distance the average neutron travels in the core and core electrolyte, in cm.	Fractional Probability of a neutron scattering with a target.	Partial Percentage of original amount of neutrons that remains.	Energy of target after collision, in MeV	Number of D-2 with an energy over 0.05 MeV as a result of this collision.	Number of hot neutrons still in the core after this scatter. (If they scatter, they are still in the core.)	Energy of hot D-2 times the number of hot D-2 at that energy.
1a	2.7450	2.283E+09	D2 in core	1.3291	8.550E+11	2.25	1.4640	0.1774	17.744	1.4159	1.5170 E +11	1.5171E+11	2.1479E+11
1a	2.7450	2.283E+09	D2 in electrolyte	1.3291	8.550E+11	2.25	1.4640	0.2200	22.004	1.4159	1.8813E+11	1.8813E+11	2.6637E +11
								MS=	39.748			3.3985E+11	
1b	2.7450	2.283E+09	Pd in Core	2.6939	8.550E+11	2.45	1.4640	0.2034	20.3372	0.0511	0	1.7388E+11	
2a	1.3291	1.589E +09	D2 in core	0.6436	3.398E+11	2.79	1.4640	0.2200	8.7450	0.6856	7.7469E +10	7.4770E+10	5.3110E+10
2a	1.3291	1.589E+09	D2 in electrolyte	0.6436	3.398E+11	2.79	1.4640	0.2729	10.8450	0.6856	9.2724E+10	9.2725E+10	6.3568E+10
								SUMS =	- 19.590			E +11	
2b	1.3291	1.589E+09	Pd in Core	1.3044	3.398E+11	4.6	1.4640	0.3818	15.1770	0.0247	0	1.2976 + 11	
2c	2.6939	2.262E+09	D2 in core	1.3044	1.7388E+11	2.27	1.4640	0.1790	3.6410	1.3895	3.126 E 10	3.13121+10	4.3251E+10
2c	2.6939	2.262E+09	D2 in electrolyte	1.3044	1.7388E+11	2.27	1.4640	0.2220	4.5150	1.3895	3.86012 + 10	3.8603E+10	5.3638E+10
								SUMS =	8.156			6.9734E+10	
2d	2.6939	2.262E+09	Pd in Core	2.6438	1.7388+11	2.4	1.4640	0.1992	4.0520	0.0501	0.0000E+00	3.4645E+10	
3a	0.6436	1.106E+09	D2 in core	0.3116	1.675E+11	2.95	1.4640	0.2326	4.5570	0.3320	3.8964 E 10	3.8962E+10	1.2934E+10
3a	0.6436	1.106E+09	D2 in electrolyte	0.3116	1.675E+11	2.95	1.4640	0.2885	5.6520	0.3320	4.8321E +10	4.8325E+10	1.6040E+10
								SUMS=	10.209			8.7287E +10	
3b	0.6436	1.106E+09	Pd in Core	0.6316	1.675E+11	7.7	1.4640	0.6392	12.5210	0.0120	0.0000E+00	1.0705E+11	
3c	1.3044	1.574E+09	D2 in core	0.6316	1.298E+11	2.8	1.4640	0.2208	3.3510	0.6728	2.8652E+10	2.8651E+10	1.9278E+10
3c	1.3044	1.574E+09	D2 in electrolyte	0.6316	1.298E+11	2.8	1.4640	0.2738	4.1560	0.6728	3.5533E+10	3.5534E+10	2.3907E +10
								SUMS =	7.507			6.4185E+10	
3d	1.3044	1.574E+09	Pd in Core	1.2801	1.298E+11	4.6	1.4640	0.3818	5.7950	0.0243	0.0000E+00	4.9547E +10	
3e	1.3044	1.574E+09	D2 in core	0.6316	6.973E+10	2.8	1.4640	0.2208	1.8010	0.6728	1.5396E+10	1.5399E+10	1.0359E+10
3e	1.3044	1.574E+09	D2 in electrolyte	0.6316	6.933E+10	2.8	1.4640	0.2738	2.2330	0.6728	1.9093E + 10	1.9092E+10	1.2846E+10
								SUMS =	4.034			3.4491E+10	
3f	1.3044	1.574E+09	Pd in Core	1.2801	6.973E+10	4.6	1.4640	0.3818	3.114	0.0243	0.0000E+00	2.6625E+10	
3g	2.6438	2.241E+09	D2 in core	1.2801	3.464E+10	2.28	1.4640	0.1798	0.7280	1.3637	6.2284E+09	6.2244E+09	8.4936E+09
3g	2.6438	2.241E+09	D2 in electrolyte	1.2801	3.464E+10	2.28	1.4640	0.2230	0.9030	1.3637	7.7240E+09	7.7207E+09	1.0533E+10
								SUMS =	1.631			1.3945E+10	
3h	2.6438	2.241+09	Pd in Core	2.5947	3.464E+10	2.45	1.4640	0.2034	0.824	0.0492	0.0000E+00	7.0452E+09	
4a	0.3116	7.694E+08	D2 in core	0.1509	8.729E+10	3.04	1.4640	0.2397	2.4470	0.1607	2.0925E+10	2.0922E+10	3.3633E+09
4a	0.3116	7.694E+08	D2 in electrolyte	0.1509	8.729E+10	3.04	1.4640	0.2973	3.0350	0.1607	2.5950E+10	2.5949E+1	4.1709E+09
												0.0000E+00	

(Continued)

Table 8. Continued

A	B	c	D	E	F	G	H	I	I	K	L	M	N
Scattering num-ber and identifier	Neutron energy before collision in MeV	Neutron velocity before collision, in cm/sec	Target of the collision	Average Neutron Energy after collision with target, in MeV	Number of hot neutrons in the core	Scattering Cross section with target, in barns, at this incident energy.	Distance the average neutron travels in the core and core electrolyte, in cm.	Fractional Probability of a neutron scattering with a target.	Partial Percentage of original amount of neutrons that remains.	Energy of target after collision, in MeV	Number of D-2 with an energy over 0.05 MeV as a result of this collision.	Number of hot neutrons still in the core after this scatter. (If they scatter, they are still in the core.)	Energy of hot D-2 times the number of hot D-2 at that energy.
4b	0.3116	7.694E+08	Pd in Core	0.3058	8.729E+10	7.5	1.4640	0.6226	6.365	0.0058	0.0000E+00	5.4421E+10	
4c	0.6316	1.095E+09	D2 in core	0.3058	1.071E+11	2.95	1.4640	0.2326	2.9128	0.3258	2.4905E+10	2.4904E+10	8.1134E+09
4c	0.6316	1.095E+09	D2 in electrolyte	0.3058	1.071E+11	2.95	1.4640	0.2885	3.6120	0.3258	3.0885E+10	3.0883E+1	1.0062E + 10
												0.0000E+00	
4d	0.6316	1.095E+09	Pd in Core	0.6198	1.071E+11	7.7	1.4640	0.6392	8.0030	0.0117	0.0000E+00	6.8426E+10	
4e	0.6316	1.095C+09	D2 in core	0.3058	6.418E+10	2.95	1.4640	0.2326	1.7460	0.3258	1.4932E+10	1.4928E+10	4.8643E+09
4e	0.6316	1.095E+09	D2 in electrolyte	0.3058	6.418E+10	2.95	1.4640	0.288	2.1660	0.3258	1.8517E +10	1.8519E+10	6.0324E+09
												0.0000E+00	
4f	0.6316	1.095E+09	Pd in Core	0.6198	6.418E+10	7.7	1.4640	0.6392	4.7980	0.0117476	0.0000E+00	4.1023E 10	
4g	1.2801	1.559 + 09	D2 in core	0.6198	4.955E+10	2.8	1.4640	0.2208	1.2800	0.6602989	1.0941E+10	1.0944E+10	7.2241E+09
4g	1.2801	1.559E+09	D2 in lectrolyte	0.6198	4.955E+10	2.8	1.4640	0.2738	1.5869	0.6602989	1.3567E +10	1.3568E+10	8.9583E+09
												0.0000E+00	
4h	1.2801	1.559E+09	Pd in Core	1.2563	4.955E+10	4.6	1.4640	0.3818	2.2128	0.0238107	0.0000E+00	1.8919E+10	
4i	0.6316	1.095C+09	D2 in core	0.3058	3.449E+10	2.95	1.4640	0.2326	0.9380	0.3257762	8.0233E+09	8.0199E+09	2.6138E+09
4i	0.6316	1.095E+09	D2 in electrolyte	0.3058	3.449E+10	2.95	1.4640	0.2885	1.1637	0.3257762	9.9500E+09	9.9500E+09	3.2415E+09
												0.0000E+00	
4j	0.6316	1.095E+09	Pd in Core	0.6198	3.449E+10	7.7	1.4640	0.6392	2.5783	0.0117476	0.0000E+00	2.2044E+10	
4k	1.2801	1.559+09	D2 in core	0.6198	2.662E+10	2.8	1.4640	0.2208	0.6880	0.6602989	5.8789E+09	5.8824E+09	3.8818E+09
4k	1.2801	1.559E+09	D2 in electrolyte	0.6198	2.662E+10	2.8	1.4640	0.2738	0.8527	0.6602989	7.2905E+09	7.2906E+09	4.8139E+09
												0.0000E+00	
4l	1.2801	1.559E+09	Pd in Core	1.2563	2.662E+10	4.6	1.4640	0.3818	1.1891	0.0238107	0.0000E+00	1.0166E+10	
4m	1.2801	1.559E+09	D2 in core	0.6198	1.395E+10	2.8	1.4640	0.2208	0.3600	0.6602989	3.0807E+09	3.0780E+09	2.0342E+09
4m	1.2801	1.559E+09	D2 in electrolyte	0.6198	1.395E+10	2.8	1.4640	0.2738	0.4468	0.6602989	3.8205E+09	3.8205E+09	2.5227E+09
												0.0000E+00	
4n	1.2801	1.559E+09	Pd in Core	1.2563	1.395E+10	4.6	1.4640	0.3818	0.6231	0.0238107	0.0000E+00	5.3276E+09	
4o	2.5947	2.220E+09	D2 in core	1.2563	7.045E+09	2.3	1.4640	0.1814	0.1490 53	1.3383258	1.2778E+09	1.2740E+09	1.7101E+09
4o	2.5947	2.220E+09	D2 in electrolyte	1.2563	7.045E+09	2.3	1.4640	0.2249		1.3383258	1.5846E+09	1.5846E+09	2.1208E+09
												0.0000E+00	
4p	2.5947	2.220E+09	Pd in Core	2.5464	7.045E+09	2.5	1.4640	0.2075	0.1710	0.0482607	0	1.4620E+09	
										Sums =	9.78499E+11		8.8300E+11
										Average energy of Hot D2 in MeV =		9.0240E-01	

column M. The number in column M goes to the next color-coded scatter, and it is seen in column F for that next color-coded scatter.

Column G is the scattering cross section, for either the ^{2}D or the palladium, in barns. Column H is the distance that the neutron travels, in the Pd or the electrolyte. Column I is the fractional probability of a scatter event occurring. In column J is the percentage, of the original amount, that still remains in the core. The probability of scattering with a ^{2}D is the sum of the probabilities of scattering with a ^{2}D in the lattice or in the electrolyte, and this sum is also shown in column J.

The kinetic energy transferred to the target is shown in column K. The number of newly energized ^{2}D is shown in column L. The number of neutrons still in the core after the scatter is shown in column M. The total number of neutrons still remaining in the core then goes to Column F, in the subsequent color-coded scatter. Column N is the product of the number of energized deuterons, times their energy, used to find the average energy.

The total number of energized deuterium is shown at the bottom of column L, as 9.78499×10^{11}, with an average energy of 0.9024 MeV. These values will be used in Section 5.

2.7. Summary of Section 2

Section 2 has given us the number and average energy of the energetic ^{2}D, which have been energized through the transference of kinetic energy from the child products of the two primary reactions: protons, ^{3}T, ^{3}He, and neutrons. These are the energized $_2$D that might potentially react in a subsequent chain reaction. These numbers will be used in Section 5 of this calculation.

Notice that the calculations for the scattering of the charged particles do not involve the palladium core size or shape. Rather, the number and energy of the scattered ^{2}D are based only on the probabilities for scattering. Furthermore, for charged particles, the only dependency on the density of the ^{2}D is in the integration limit for the probabilities, resulting in only a very weak ^{2}D density dependency.

However, for the ^{2}D scattering with neutrons, there is a directly proportional dependency on sample shape, size, and deuterium density. Thus, any LENR reactor configuration that ignores the neutrons–and how best to contain the neutron energy–is missing a significant contribution to the reactor's energy production. Quoting directly from [8]:

"We then demonstrate the superior efficiency of the kinetic energy transfer by energetic neutrons on the target deuteron nuclei, resulting in subsequent nuclear reactions. Such a process is a key ingredient in achieving and sustaining nuclear reactions."

3. Calculate the Reaction Rate of the Secondary Reactions ^{3}T+^{2}D and ^{3}He+^{2}D

In Section 3 of this example calculation, the following calculations and observations will be made.

a. Understanding the Reaction Rate Calculations
b. Calculate the average projectile distance between scatters, L_{ave}.
c. Calculate the average number, N_{ave}, of scattering events that occur before the energy drops to the next lower level.
d. Examine the dependency of the $L_{ave} \times N_{ave}$ product on angle.
e. Calculate the reaction rate of the secondary1 reaction, ^{3}T+^{2}D−>^{4}He+n.
f. Calculate the reaction rate of the secondary2 reaction, ^{3}He+^{2}D−>^{4}He+p.
g. Summary of section 3.

3.1. Understanding the Reaction Rate Calculations

The reaction rate for fusion reactions can be calculated by using the Lawson equation [38], shown in Eq. (37).

$$\mathrm{fusion}_{\mathrm{rate}} = (\rho_{\mathrm{target}})\,(\sigma\,(E))\,(v_{\mathrm{projectile}})\,(\rho_{\mathrm{projectile}}) \tag{37}$$

where:

$fusion_{rate}$ is the fusion rate

ρ_{target} is the target density in number per cm^3

σ(E) is the reaction cross section in cm^2, and it is a function of energy

$v_{projectile}$ is the velocity of the projectile, (assuming the target velocity is negligibly small in comparison.)

$\rho_{projectile}$ is the projectile density in units of number per cm^3.

In order to calculate this reaction rate for our example calculation, we must know all four of these factors. We know the density of the ^{2}D target. We know the energy of the projectile and, therefore, its velocity. We know the reaction cross section as a function of energy, σ(E), from experimental data for the reaction. The difficult parameter to determine, in this equation, is the density of the energetic projectiles, ^{3}T and ^{3}He, as a function of projectile energy, ρ(E). To determine this requires an involved calculation.

For a particular energy range, the projectile density will be the introduction rate at this energy, multiplied by the amount of time spent at this energy, as seen in Eq. (38).

$$\rho_{\mathrm{projectile}} = \mathrm{Rate}_{\mathrm{intro}}(E) \times t_{projectile\_at\_energy} \tag{38}$$

where:

$\rho_{projectile}$(E) is the projectile density as a function of the projectile energy.

$t_{projectile\_at\_energy}$ is the time that the projectile stays within a particular energy range E.

For our example, the initial introduction rate of 8.55×10^{11} projectiles/sec is only true for the original energy of the projectiles upon their emission from the primary reactions. As the projectiles scatter within their environment, the average energy of the projectiles will decrease, and as the energy decreases, the reaction cross section also changes. When the energetic projectiles step down from their original energy to a lower energy, they either collide, escape the core, or react. Thus, the introduction rate for a particular energy interval will also decrease, as the average energy of the projectiles decreases. For this example calculation, the energy will be stepped down in intervals of 0.1 MeV.

The calculations for scattering are useful in making this determination. During the time that the projectile energy is within a particular energy interval, there is a scattering cross section for that energy, an average energy loss per scatter, and an average distance traveled for that energy. We subtract out the number of projectiles that escape the core or react. We repeat this calculation for the next energy step, and reiterate this procedure until the energy is too low for further reactions. In this manner, we are able to solve for the introduction rate as a function of energy, for use in Eq. (38). Once the introduction rate and the distance traveled are known for a given energy range, we are able to solve for the average projectile density, at that given energy range.

We have to determine how much time the average projectile stays within this energy interval. To calculate the time spent, we need to know the distance the average projectile will travel before it decreases its energy into the next lower energy. The time that a projectile spends in the core is the distance travelled by the projectile divided by its velocity, as seen in Eq. (39).

$$t_{projectile\_in\_core} = \frac{\mathrm{Distance}_{projectile-in-core}}{v_{projectile\_E1}} \tag{39}$$

Combining Eq. (37), (38), and (39) yields Eq. (40).

$$\mathrm{fusion}_{\mathrm{rate}} = (\rho_{\mathrm{target}})\,(\sigma\,(E))\,(\mathrm{Rate}_{\mathrm{intro}})\,(\mathrm{Distance}_{projectile\_in\_core}) \tag{40}$$

where:

ρ_{target} is the density of the cold deuterium fuel

$Distance_{projectile-in-core}$ is the same as the total distance, $\text{distance}_{\text{total}}$, travelled within that energy range.

Note that in Eq. (40), the projectile velocity, and we are left only needing to know the total distance travelled by the projectile before it either escapes the core or loses its energy.

The scattering concepts previously discussed are an important part of this calculation. We need to know the average distance that a projectile travels within the reactor core before it loses its energy. In order to determine this average distance, we need to know not only the average number of times it scatters, but also the average distance, L_{ave}, between each scatter. The average distance between scatters is the average distance between the deuterium. If the density of deuterium, in number per cubic centimeter, is $\rho_{deuterium}$, then the average distance between the target deuterium is the reciprocal the cubed root of this density, as shown in Eq. (41).

$$L_{\text{ave}} = \left(\frac{1}{\sqrt[3]{\rho_{\text{deuterium}}}} \right) \tag{41}$$

To calculating the total distance, $\text{distance}_{\text{total}}$, traveled by the projectile, we must take this average distance between collisions, L_{ave}, and multiply it by the average number of collisions N that occurs before the energetic projectile loses its energy to the next lower energy range.

$$\text{distance}_{\text{total}} = L_{\text{ave}} \times N \tag{43}$$

The number of collisions N was determined previously with Eq. (34). For this paper, the distance is the net distance traveled, taking into consideration the scattering of the projectile with the ^{2}D and the Pd.

For an LENR reactor, the L_{ave} × N product is determined for each energy interval from the very first original energy down to the lowest energy threshold. This value $distance_{total}$ can then be used in Eqs. (37–40) to find the reaction rate f_E for each energy interval. This reaction rate is then summed for all energies.

By stepping the energy down through its entire energy range, using an energy step ΔE of 0.1 MeV, the total fusion rate, $fusion_{total}$, is the sum of all the fusion rates at each energy interval, as in Eq. (44).

$$\text{fusion}_{\text{total}} = \sum_{E_i = E_{\text{highest}}}^{E_{\text{lowest}}} \text{fusion}_{rate\_E_i} \quad (in\ steps\ of \Delta E) \qquad (44) \tag{44}$$

Using these numbers and equations, we can solve for the reaction rates. This calculation of reaction rates is done for both the ^{3}T + ^{2}D and the ^{3}He + ^{2}D reactions.

3.2. Calculate the Reaction Rate of the Secondary1 Reaction, ^{3}T+^{2}D−>^{4}He+n

The original energy upon emission of the ^{3}T nuclide is 1.01 MeV, in the lab reference frame. Adding in the extra amount of energy from the previous projectile, as is correct to do, this energy is 1.11 MeV; in the center-of-mass reference frame, this converts to a center-of-mass energy of 0.44 MeV.

The lowest energy, for which a reaction might reasonably occur, can be selected from the experimental cross section charts of the ^{3}T to ^{2}D reaction, shown in Fig 5. Note that these cross sections in Figure 7 use the center-of-mass kinetic energy, E_{CM}.

As can be seen from Figure 7, the reaction cross section is too low to be important at about 0.01 MeV for the center-of-mass energy, with a cross section of 0.03 barns, indicated in Figure 7 by the red arrow. This center-of-mass energy of 0.01 MeV (0.025 MeV lab reference frame) is used as the lowest energy to consider. Thus, the center-of-mass energy range for consideration is from 0.440 MeV to 0.01 MeV.

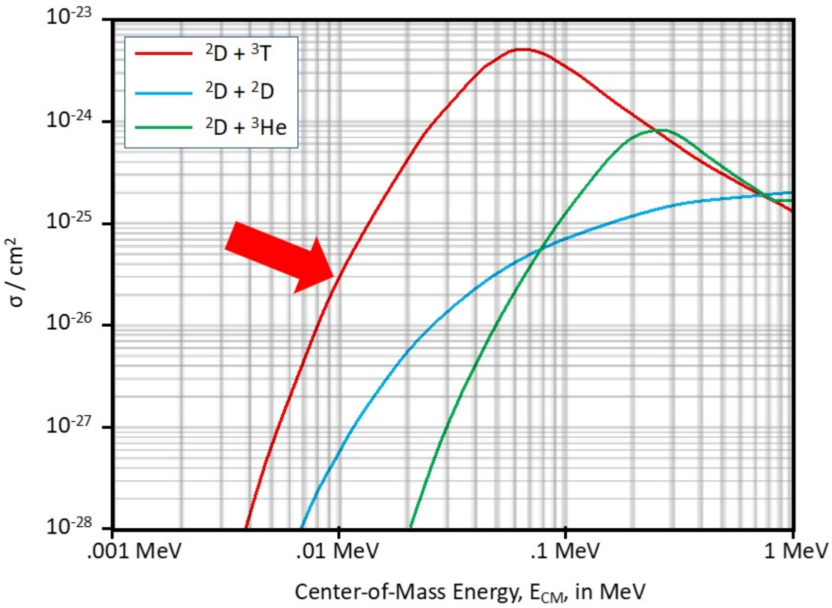

Figure 7. Reaction cross sections for three reactions.

Let us now calculate the reaction rates for the ^{3}T to ^{2}D reaction for this first original energy interval, using Eq. (40). The average distance traveled by the projectile before losing energy to the next energy step is 0.05437 cm, as shown in Table 9, for the laboratory energy interval of 1.11 to 1.1 MeV. The projectile of ^{3}T has an initial laboratory energy of 1.01 MeV, which is 0.44 MeV in the center-of-mass reference frame, and at this energy, it has a reaction cross section of 3.60×10^{-25} cm^2. For our example, the density of the ^{2}D is 5.387×10^{22}, and the introduction rate for the triton projectiles is 8.55×10^{11} for the entire sample. Using these numbers in Eq. (40) gives a reaction rate, for this one energy range, of 9.015×10^8, as shown in Calc. 2.

$$\text{fusion}_{\text{rate}} = \left(5.387 \times 10^{22}\right)\left(3.6 \times 10^{-25}\right)\left(8.55 \times 10^{11}\right)(0.05437) = 9.015 \times 10^8 \tag{Calc. 2}$$

This is the reaction rate that will occur for the projectile energies being between 1.11 to 1.1 MeV laboratory reference frame. This amount of ^{3}T is subtracted from the number of ^{3}T projectiles that are in the core. Also, any projectiles that escape the core are also a loss in the number of excited ^{3}T projectiles as well, estimated to be 0.1% for each energy range in the calculation. (Very few charged particle ion projectiles will escape the core. Rather they will tend to get caught inside the core and either become interstitial particles within the lattice. Or after they loss all their kinetic energy, they may combine with another hydrogen atom, and escape the lattice as a room-temperature molecule of gas.) This leaves a remainder of projectiles, of $(8.55 \times 10^{11} - 9.015 \times 10^8 - 8.55 \times 10^8) = 8.53 \times 10^{11}$ energetic ^{3}T that remain in the core, at a laboratory reference frame energy of 1.10 MeV. These values are shown in the first row of Table 9. They continue scattering and reacting, as shown in Table 9.

In Table 9, the value in column A is the initial laboratory energy for that energy step. Column B shows the introduction rate of projectiles for that energy. For the first row, it is 8.55×10^{11}. For the following rows, the value in column B is the same as the value in column J for the row above. Column C is the laboratory velocity at that laboratory energy. Column D is the average distance travelled in centimeters, for that laboratory energy range. Column E is

Table 9. Reaction rates for ^{3}T to ^{2}D, for the reaction energy from the original energy of 1.11 MeV, going down to the lower threshold limit of 0.01 MeV.

A	B	C	D	E	F	G	H	I	J
Laboratory Energy of projectile ion in MeV	Introduction rate of projectile ion in #/cm^3/sec	Projectile velocity at this energy in cm/sec	Average distance traveled in cm, $L \times N$, for this energy	Relative Center-of-Mass Energy in MeV	Reaction cross section at this center-of-mass energy, in cm^2	Reaction rate at this energy for the 2.4 cm^3 loaded sample	Fraction of lost of projectiles, by reaction	Estimated % of lost projectiles, by escape	Amount of T-3 remaining in core, when the energy drops to next level
1.11	8.55E+11	8.42E+08	0.054371787	0.44	3.60E-25	9.015E+08	1.054E-03	0.1%	8.53E+11
1.1	8.53E+11	8.38E+08	0.424248336	0.44	3.60E-25	7.019E+09	8.227E-03	0.1%	8.45E+11
1	8.45E+11	7.99E+08	3.4750E-01	0.40	4.10E-25	6.488E+09	7.674E-03	0.1%	8.38E+11
0.9	8.38E+11	7.58E+08	3.4750E-01	0.36	4.60E-25	7.216E+09	8.610E-03	0.1%	8.30E+11
0.8	8.30E+11	7.15E+08	3.9396E-01	0.32	5.70E-25	1.004E+10	1.210E-02	0.1%	8.19E+11
0.7	8.19E+11	6.69E+08	3.5475E-01	0.28	7.00E-25	1.096E+10	1.338E-02	0.1%	8.07E+11
0.6	8.07E+11	6.19E+08	2.0567E+00	0.24	8.30E-25	7.424E+10	9.195E-02	0.1%	7.32E+11
0.5	7.32E+11	5.65E+08	1.8540E+00	0.20	1.19E-24	8.704E+10	1.188E-01	0.1%	6.45E+11
0.4	6.45E+11	5.05E+08	1.9257E+00	0.16	1.84 E -24	1.231E+11	1.909E-01	0.1%	5.21E+11
0.3	5.21E+11	4.38E+08	1.6452E-01	0.12	2.60E-24	1.201E+10	2.304E-02	0.1%	5.09E+11
0.29	5.09E+11	4.30E+08	1.7029E-01	0.12	2.60E-24	1.213E+10	2.385E-02	0.1%	4.96E+11
0.28	4.96E+11	4.23E+08	1.6930E-01	0.11	3.08E-24	1.393E+10	2.809E-02	0.1%	4.82E+11
0.27	4.82E+11	4.15E+08	1.7570E-01	0.11	3.08E-24	1.404E+10	2.915E-02	0.1%	4.67E+11
0.26	4.67E+11	4.07E+08	1.7603E-01	0.10	3.56E-24	1.577E+10	3.376E-02	0.1%	4.51E+11
0.25	4.51E+11	4.00E+08	1.7739E-01	0.10	3.56E-24	1.534E+10	3.402E-02	0.1%	4.35E+11
0.24	4.35E+11	3.92E+08	1.8494E-01	0.10	3.56E-24	1.543E+10	3.546E-02	0.1%	4.19E+11
0.23	4.19E+11	3.83E+08	1.9317E-01	0.09	3.80E-24	1.658E+10	3.954E-02	0.1%	4.02E+11
0.22	4.02E+11	3.75E+08	2.0215E-01	0.09	3.80E-24	1.665E+10	4.138E-02	0.1%	3.85E+11
0.21	3.85E+11	3.66E+08	2.1202E-01	0.08	4.28E-24	1.883E+10	4.888E-02	0.1%	3.66E+11
0.2	3.66E+11	3.57E+08	2.2290E-01	0.08	4.28E-24	1.881E+10	5.139E-02	0.1%	3.47E+11
0.19	3.47E+11	3.48E+08	1.9527E-01	0.08	4.28E-24	1.562E+10	4.502E-02	0.1%	3.31E+11
0.18	3.31E+11	3.39E+08	2.0644E-01	0.07	4.76E-24	1.752E+10	5.293E-02	0.1%	3.13E+11
0.17	3.13E+11	3.29E+08	2.1896E-01	0.07	4.76E-24	1.758E+10	5.614E-02	0.1%	2.95E+11
0.16	2.95E+11	3.20E+08	2.3309E-01	0.06	4.80E-24	1.779E+10	6.027E-02	0.1%	2.77E+11
0.15	2.77E+11	3.10E+08	2.4918E-01	0.06	4.80E-24	1.786E+10	6.443E-02	0.1%	2.59E+11
0.14	2.59E+11	2.99E+08	2.4862E-01	0.06	4.80E-24	1.665E+10	6.428E-02	0.1%	2.42E+11
0.13	2.42E+11	2.88E+08	2.6853E-01	0.05	4.00E-24	1.401E+10	5.786E-02	0.1%	2.28E+11
0.12	2.28E+11	2.77E+08	2.9191E-01	0.05	4.00E-24	1.433E+10	6.289E-02	0.1%	2.13E+11
0.11	2.13E+11	2.65E+08	2.0644E-01	0.04	2.20E-24	5.220E+09	2.446E-02	0.1%	2.08E+11
0.1	2.08E+11	2.53E+08	2.2821E-01	0.04	2.20E-24	5.623E+09	2.704E-02	0.1%	2.02E+11
0.09	2.02E+11	2.40E+08	1.7905E-01	0.04	2.20E-24	4.288E+09	2.122E-02	0.1%	1.98E+11
0.08	1.98E+11	2.26E+08	2.0299E-01	0.03	1.09E-24	2.355E+09	1.192E-02	0.1%	1.95E+11
0.07	1.95E+11	2.11E+08	1.7431E-01	0.03	1.09E-24	1.996E+09	1.023E-02	0.1%	1.93E+11
0.06	1.93E+11	1.96E+08	1.6008E-01	0.02	3.00E-25	4.990E+08	2.587E-03	0.1%	1.92E+11
0.05	1.92E+11	1.79E+08	1.2960E-01	0.02	3.00E-25	4.025E+08	2.094E-03	0.1%	1.92E+11
0.04	1.92E+11	1.60E+08	6.7682E-02	0.02	3.00E-25	2.096E+08	1.094E-03	0.1%	1.91E+11
0.03	1.91E+11	1.38E+08	5.5539E-02	0.01	2.00E-27	1.144E+06	5.983E-06	0.1%	1.91E+11
0.02	1.91E+11	1.13E+08	5.0995E-02	0.01	2.00E-27	1.049E+06	5.494E-06	0.1%	1.91E+11
0.01									
					Sum =	6.4841E+11			
					Percentage of T-3 that reacts =	75.84			

the relative center-of-mass energy for that same laboratory energy. Column F is the reaction cross section for that center-of-mass energy, obtained from experimental data for this reaction. The reaction rate is given in column G, as per Eq. (37), using an averaged velocity to determine the time spent in the core. The fractional loss due to reaction of the number of projectiles is shown in column H, and the percentage loss of the number of projectiles due to escape is estimated at 0.1%, shown in column I. Column J is the amount of tritium remaining after loss and reactions. This value in column J goes on to column B for the next row down.

At the bottom of Column G is the summation of the number of ^{3}T to ^{2}D reactions per second, per cm^3. For this example, that reaction rate is 6.4841×10^{11}, or 75.84%.

Experimentally, it is known that the energy released by the ^{3}T+^{2}D reaction is 17.59 MeV per reaction, with 3.518 MeV going to the ^{4}He and 14.072 going to the neutron. Recall that there is one watt of energy from the two primary reactions for this example. Under those conditions, the energy released by this secondary reaction is $(0.7584)(8.55 \times 10^{11})(17.59\ \text{MeV}) = 1.1406 \times 10^{13}\ \text{MeV} = 1.827$ watts. For this example calculation, there are 6.484×10^{11} particles of ^{4}He emitted from this secondary reaction at an energy of 3.581 MeV, and there are 6.484×10^{11} neutrons emitted at 14.072 MeV. These values are used in Section 5 of this calculation.

3.3. Calculate the Reaction Rate of the Secondary2 Reaction, ^{3}He+^{2}D−>^{4}He+p

Let us continue to calculate the reaction rate for the secondary2 reaction. The calculations are similar to those used for Section 3.2.

As before, the density of the target ^{2}D is 5.387×10^{22} per cm^3, and the initial introduction rate is 8.55×10^{11} for the sample. The ^{3}He ion is emitted with the very first initial laboratory energy of 0.8175 MeV. Adding in the average kinetic energy of the previous reaction, this becomes 0.915 MeV, in the laboratory reference frame. Using this value for the original laboratory energy, with an energy interval of 0.915 to 0.9 MeV, the average distance traveled by the projectile, for all possible angles at the first energy step, is 0.1222 cm. In the center-of-mass reference frame, this energy is 0.370 MeV. For this center-of-mass energy, the reaction cross section is obtained from the green curve in Figure 7. The reaction cross section at a center-of-mass energy of 0.370 MeV is 5.8×10^{-25} cm^2.

Using these numbers in Eq. (40) gives a fusion reaction rate of 6.412×10^9, as shown in Calc. 3.

$$f = \left(5.387 \times 10^{22}\right)\left(5.8 \times 10^{-25}\right)\left(8.55 \times 10^{11}\right)(0.1222) = 3.263 \times 10^9 \qquad \text{(Calc. 3)}$$

This is the reaction rate that occurs for the projectile laboratory energies between 0.915 to 0.9 MeV. This amount is subtracted from the number of ^{3}He projectiles that are in the core. Also any projectiles that escaped the core is a loss in the number of ^{3}He projectiles as well; as before, we estimate this number with a value of 0.1%. Thus for the projectiles between the laboratory energy range of 0.915 to 0.9 MeV, there will be a loss of 3.263×10^9 due to reaction, and 8.55×10^8 due to the excited ^{3}He escaping the core. This leaves the remaining excited ^{3}He projectiles, 8.53×10^{11}, which are now at an energy of 0.9 MeV. These values are shown in the row 1 of Table 10. These remaining projectiles continue scattering and reacting, as shown in the remaining rows of Table 10.

In Table 10, the description of the information for each column is similar to Table 9. The number of the ^{3}He that react is 1.893×10^{11}, which is 22.140%, highlighted in greed at the bottom of column G. The remainder of these ^{3}He particles simply stay in the core, and eventually escape as low energy ^{3}He.

The energy released by the ^{3}He+^{2}D reaction is 18.40 MeV per reaction with 3.680 MeV going to the ^{4}He and 14.720 MeV going to the proton. The power released by this secondary reaction is:

$$(0.2214)(8.55 \times 10^{11})(18.40) = 3.483 \times 10^{12}\ \text{MeV/sec} = 0.5580\ \text{watts}.$$

For this example, there are 1.893×10^{11} of protons and ^{4}He particles emitted by this secondary2 reaction. These values will be used in Section 5.

Table 10. Reaction rates for ^{3}He to ^{2}D, for the full reaction going from initial energy of 0.915 down to the lower limit of energy for a reaction, 0.07 MeV.

A	B	C	D	E	F	G	H	I	J
Laboratory Energy of projectile ion in MeV	Introduction rate of projectile ion in #/cm^3/sec	Projectile velocity at this energy in cm/sec	Average distance traveled in cm, L × N, for this energy	Relative Center-of-Mass Energy in MeV	Reaction cross section at this center-of-mass energy, in cm^2	Reaction rate at this energy for the 2.4 cm^3 loaded sample	Fraction of lost of projectiles, by reaction	Estimated % of lost projectiles, by escape	Amount of He-3 remaining in core, when the energy drops to next level
0.915	8.55E+11	7.64E+08	0.1222	0.37	5.80E-25	3.263E+09	1.59E-03	0.1%	8.53E+11
0.9	8.53E+11	7.58E+08	0.8818	0.36	6.00E-25	2.430E+10	1.19E-02	0.1%	8.42E+11
0.8	8.42E+11	7.15E+08	0.8938	0.32	7.10E-25	2.878E+10	1.42E-02	0.1%	8.29E+11
0.7	8.29E+11	6.69E+08	0.8818	0.28	7.80E-25	3.071E+10	1.54E-02	0.1%	8.15E+11
0.6	8.15E+11	6.19E+08	0.8848	0.24	8.30E-25	3.225E+10	1.65E-02	0.1%	8.01E+11
0.5	8.01E+11	5.65E+08	0.9697	0.2	7.00E-25	2.929E+10	1.52E-02	0.1%	7.88E+11
0.4	7.88E+11	5.05E+08	1.1133	0.16	4.70E-25	2.221E+10	1.17E-02	0.1%	7.78E+11
0.3	7.78E+11	4.38E+08	1.4644	0.12	2.40E-25	1.473E+10	7.89E-03	0.1%	7.71E+11
0.2	7.71E+11	3.57E+08	1.5013	0.08	6.00E-26	3.742E+09	2.02E-03	0.1%	7.69E+11
0.1	7.69E+11	2.53E+08	0.0612	0.04	4.00E-27	1.014E+07	5.49E-06	0.1%	7.68E+11
0.09	7.68E+11	2.40E+08	0.0576	0.04	4.00E-27	9.534E+06	5.17E-06	0.1%	7.67E+11
0.08	7.67E+11	2.26E+08	0.0560	0.03	1.00E-27	2.315E+06	1.26E-06	0.1%	7.67E+11
0.07	7.67E+11	2.11E+08	0.0496	0.03	1.00E-27	2.050E+06	1.11E-06	0.1%	7.66E+11
					Sum =	1.893E+11			
					Percentage =	22.140	%		

3.4. Summary of Section 3

For an LENR reactor described in this example, the total additional energy released from the two secondary reactions for this example is $1.827+ 0.5580 = 2.384$ watts. This is in addition to the 1 watt of power already being produced by the primary reactions. Thus, these secondary reactions actually produce a relatively large amount of power, more than the primary reactions. The total power output of the reactor is 3.384 watts, a reasonable value for a reactor core size of 2.4 cm^3 of loaded palladium. The total number of ^{4}He nuclei emitted is 8.377×10^{11} per second.

4. Calculate Scattering Rates of Energetic Child Products from Secondary Reaction

This section will proceed as follows.

4.1 Calculate scattering rate of the energetic ^{4}He ions from secondary1 reaction.
4.2 Calculate scattering rate of energetic neutrons from secondary1 reaction.
4.3 Calculate scattering rate of the energetic ^{4}He ions from secondary2 reaction.
4.4 Calculate scattering rate of the energetic protons from secondary2 reaction.
4.5 Summary of section 4.

4.1. Calculate the Scattering Rate of the Energetic ^{4}He from Secondary1 Reaction

These calculations in Section 4 are similar to the calculations in Section 2 for scattering. The total energy released from the secondary1 reaction is 17.590 MeV, plus an average of 0.20 MeV for the incoming projectile. Thus, for an average ^{4}He initially released from secondary1 reaction, it has an initial kinetic energy of 3.558 MeV. Similar to the other projectiles, we want to know how many of these ^{4}He projectiles are going to collide with a ^{2}D atom inside the core, transferring a sufficient amount kinetic energy to the ^{2}D, such that a ^{2}D+^{2}D reaction might occur. To do this, we use the scattering techniques described in Section 2. We use the mass number A = 4 for the ^{4}He projectile, with the initial first energy of 3.558 MeV. At this energy, the initial deflection angle must be 14° in order to give the cold ^{2}D enough energy, 0.05 MeV, such that it might react. Similar to the calculations in Tables 4, 5, and 6, done in Section 4, this calculation is iterated for every energy range from the very first initial energy down to the lowest energy to be considered. (Due to the similarity of the previous tables, the table is not repeated here.) The result of these calculations for the scattering of ^{4}He from the secondary1 reaction with ^{2}D show that there are 6.0277×10^{12} successful scattering events, and the average energy of these successfully scattered ^{2}D is 0.1760 MeV. These numbers will be used in Section 5.

4.2. Calculate Scattering Rate of the Energetic Neutrons from Secondary1 Reaction

These calculations are similar to the neutron scattering from Section 2.5, but starting at a higher initial energy of 14.232 MeV. (This value includes 0.2 MeV from the incoming projectile of the previous reaction.) As before, the scattering neutron cross section is read from the experimental data plots [36], [37]. As previously done, Eqs. (12) and (36) are used to determine the number of neutrons that scatter with a ^{2}D in a successful collision. Specifically, we will use the average fraction of retained energy after one scatter for the neutron for a collision with ^{2}D of 48.42%, and for a collision with ^{106}Pd of 98.14%. Similar to the branching calculation shown in Figure 6 and Table 8, this is done for the neutrons that are the child by-products of secondary1 reaction.

The calculation for the first original energy will be done here. The energy released from the secondary2 reaction is 17.590 MeV, plus an average of 0.20 MeV for the incoming projectile. Thus for an average neutron initially released from secondary1 reaction, it has an initial kinetic energy of 14.232 MeV, which is a velocity 5.20×10^9 cm/second. Its scattering cross section is 0.685 barns.

As before, the average distance it travels in the Pd core 1.424 cm. The density of the target ^{2}D particles is 5.387 × 10^{22}. Using these numbers gives the fractional probability of scattering to be 0.0499%, as shown in Calc. 4.

$$P_{n\_to\_d} = \left(0.685 \times 10^{-24}\right)(1.424)\left(5.387 \times 10^{22}\right) = .0525 \qquad \text{(Calc. 4)}$$

Initially, the number of neutrons produced from the secondary1 reaction is the amount of 6.484 × 10^{11} neutrons per second, (as determined in Section 3.2.), each with an initial energy of 14.232 MeV. From Calc. 4, we see that the fractional probability that they will scatter with a ^{2}D is 0.0525, or 5.25%. These neutrons can scatter either with the ^{2}D in lattice or with the ^{2}D in the electrolyte, or with the palladium atoms in the metal lattice.

As was done previously in Section 4.5 using Tables 7 and 8, when scattering with deuterium either in the lattice or the electrolyte, the neutrons will retain an average of 0.4842 of their energy. For these higher energy neutrons from the secondary1 reaction, at an original energy of 14.232 MeV, this means that an energy of 14.232 × 0.4842 = 6.891 MeV is retained by the average neutron, and it transfers 14.232−6.891 = 7.341 MeV of energy to the ^{2}D. Similarly, for a neutron scattering with palladium, the average neutron will retain an average of 0.9814 of its energy, (which is 14.232 × 0.9814 = 13.967 MeV), and it transfers 14.232−13.967 = 0.2647 MeV to the palladium atom.

Detailed calculations, similar to those shown in Table 8, are done. However, due to the similarity of these calculations, this very large table is not shown here. The initial number of energetic neutrons and the very first initial starting energy of these neutrons are different, but the calculations and pattern are the same. For an original amount of 6.484 × 10^{11} neutrons with an initial energy of 14.232 MeV, the final result of this iterative calculation is that 2.2635 × 10^{11} deuterons are energized above 0.05 MeV, with an average energy of 5.1178 MeV of energy. These are the deuterons per second that could potentially react with another cold deuteron in a subsequent reaction. We will use these numbers in Section 5.

4.3. Calculate Scattering Rate of the Energetic ^{4}He from Secondary2 Reaction

This is similar to what was done in Section 4.1, but with a slightly higher first initial energy. The total energy released from the secondary2 reaction is 18.40 MeV, plus an average of 0.20 MeV for the incoming projectile. The ^{4}He child products of secondary2 reaction have a kinetic energy of 3.720 MeV upon their release from the secondary2 reaction. The number of ^{4}He released as a child product of the secondary2 reaction is 1.893 × 10^{11}, as determined previously.

For the ^{4}He from the secondary2 reactions, the result of the scattering calculation is 1.846 × 10^{12} energized ^{2}D, with an average energy of 0.17725 MeV. (Due to the similarity of the previous tables, this table is not repeated here.) These are the deuterons that could potentially react with another cold deuteron in a subsequent reaction. We will use these numbers in Section 5.

4.4. Calculate Scattering Rate of the Energetic Protons from Secondary2 Reaction

The total energy released from the secondary2 reaction is 18.40 MeV, plus an average of 0.20 MeV for the incoming projectile. The emitted protons from of secondary2 reaction have a kinetic energy of 14.88 MeV upon their release from the secondary2 reaction. The number of protons released from the secondary2 reaction (as calculated previously) is 1.893 × 10^{11}. Similar to the other projectiles we have considered thus far, these proton projectiles scatter with a ^{2}D atom inside the reactor core, some of which transfer a sufficient amount kinetic energy to the ^{2}D for a possible subsequent ^{2}D+^{2}D reaction. With these values, the calculations are similar to what was done previously, but they are not shown. The results are that 7.658 × 10^{12} ^{2}D are successfully scattered, with an average energy of 0.2255 MeV. These are the energetic deuterons could potentially react with another cold deuteron in a subsequent reaction. We will use these numbers in Section 5.

Table 11. The compilation of all the energized deuterium that are energized to a value of over 0.05 MeV, for all eight child products.

A	B	C	D	E
Projectile	Source of projectile	Number of energized D-2 produced from this projectile	Average energy in MeV for this energized D-2	Number of energized D-2 times average energy of D-2
Proton	Primary1	7.4027E+12	0.20591	1.524E+12
T3	Primary1	2.0155E+12	0.13109	2.642E+11
Neutron	Primary2	9.7850E+11	0.90240	8.830E+11
He3	Primary2	1.6982E+12	0.12537	2.129E+11
He4	Secondary1	6.0278E+12	0.17602	1.061E+12
Neutron	Secondary1	2.2635E+11	5.11776	1.158E+12
He4	Secondary2	1.8458E+12	0.17725	3.272E+11
Proton	Secondary2	7.6581E+12	0.22547	1.727E+12
	Sum =	2.7853E+13		7.158E+12
	Average energy of energized D-2, in MeV =		0.2570	

4.5. Summary of Section 4

From the four child products of secondary1 and secondary2 reactions, the number of resulting energetic ^{2}D, due to collisions with these child products, has been determined, using charged-particle scattering techniques and neutron scattering techniques, described previously. For each of these four child products, we have determined the number of energetic ^{2}D particles that are at an energy of 0.05 MeV or higher.

5. Part 4 of the Example Calculation: Determination of a Chain Reaction

This section will proceed as follows:

7.1 Add up the energetic ^{2}D in the reactor core from all eight child products.

7.2 Calculate the reaction rate for this subsequent ^{2}D to ^{2}D reaction.

5.1. Add up the Energetic ^{2}D in the Reactor Core, from all Eight Child Products

From the eight child products and their scattering rates as determined in Sections 2 and 4, these values are shown in Table 11.

As can be seen in Table 11, the child products of the preceding ^{2}D to ^{2}D primary reactions and the secondary reactions energize a total of 2.3031×10^{13} deuterons, at an average energy of 0.4616 MeV, in the lab energy reference frame. In order to determine the reaction rate of the subsequent ^{2}D to ^{2}D reaction, due to these energized deuterons, each ^{2}D energy range is considered individually.

5.2. Calculate the Reaction Rate of the Energized ^{2}D in a Subsequent ^{2}D+^{2}D Reaction

Since the cross sections shown in Figure 7 use the center-of-mass reference frame, the energy ranges are first converted to center-of-mass energies, then the calculations are done. The resulting reaction rates are calculated, similarly to what was done previously in Section 5. The results are shown in Table 12.

The cross-section tables are not a linear function with respect to energy. Because of this, it is inaccurate to take the average energy of the total number of the hot ^{2}D and the total number of the energized ^{2}D, and do a simple calculation

Table 12. The reaction rates for the subsequent hot ^{2}D to cold ^{2}D reaction, only for the hot ^{2}D projectiles energized from the protons of primary1 reaction.

A	B	c	D	E	F	G	H
Lab energy range of projectile ion, in MeV	Introduction rate of projectile ion in #/cm^3/sec	Average total distance travelled before the energy drops to next level, in cm.	Reaction cross section at this energy, in cm^2.	Reaction rate at this energy for the entire 2.4 cm^3 sample	The fraction of the lost projectiles due to reaction.	Percentage of the lost projectiles due to escape.	Amount of energetic D-2 remaining in NAE after the energy drops to next level.
0.2059	7.403E+12	2.80	8.900E-26	9.929E+10	5.59E-03	0.001	7.354E+12
0.200	7.354E+12	3.61	7.200E-26	1.029E+11	5.83E-03	0.001	7.304E+12
0.150	7.304E+12	3.95	5.200E-26	8.071E+10	4.60E-03	0.001	7.263E+12
0.1	7.263E+12	5.18	3.200E-26	6.490E+10	3.72E-03	0.001	7.229E+12
0.05	7.229E+12	0	9.500E-27	0.000E+00		0.001	7.221E+12
			Sum =	3.478E+11			

Table 13. The hot ^{2}D to cold ^{2}D reaction rates for all of the hot ^{2}D projectiles from all eight child products of the preliminary ^{2}D to ^{2}D reactions. This total value must be greater than 1.71E+12 for a chain reaction to occur.

A	B	C	D
Reaction	Source of D2 projectile	Number of hot D2	D2 to D2 Reaction rate
hot D2 to cold D2	D2 Scattered from Proton from Primary1	7.4027E+12	3.4778E+11
hot D2 to cold D2	D2 Scattered from T3 from Primary1	2.0155E+12	4.0182E+10
hot D2 to cold D2	D2 Scattered from Neutron from Primary2	9.7850E+11	2.8785E+11
hot D2 to cold D2	D2 Scattered from He3 from Primary2	1.6982E+12	3.3855E+10
hot D2 to cold D2	D2 Scattered from He4 from Secondary1	6.0278E+12	6.2368E+10
hot D2 to cold D2	D2 Scattered from Neutron from Secondary1	2.2635E+11	4.5522E+11
hot D2 to cold D2	D2 Scattered from He4 from Secondary2	1.8458E+12	2.0367E+11
hot D2 to cold D2	D2 Scattered from Proton from Secondary2	7.6581E+12	3.5978E+11
	Sums =	2.785E+13	1.7907E+12
		Percentage of hot D-2 that react =	6.43%

for the subsequent reaction rate. Instead, a more accurate method is to take the number of energetic ^{2}D for each energy range, and calculate the resulting reaction rate for that energy and number. This is how the calculation proceeds, using all eight energy ranges from all eight child products shown in Table 11, starting with the energized ^{2}D resulting from collisions with the proton of primary1 reaction. The table is showing the reaction rate for ^{2}D to ^{2}D reactions.

The descriptions of the columns and numbers shown in Table 12 are similar to those of Tables 9 and 10. As can be seen in the boxes highlighted in green, there are 3.47×10^{11} reactions for these hot ^{2}D projectiles.

This same calculation, as shown in Table 12, is done for all of the eight rows of Table 11. Due to the similarity of these other seven table to Table 12, these other tables are not be shown in detail. Table 13 shows the resulting summation of the reaction rate, for all eight rows of Table 11.

Column A is the reaction type. For all of these, it is hot ^{2}D interacting with the cold ^{2}D. The source of the energized ^{2}D is listed in column B, as being the ^{2}D that resulted from the scattering from one of the eight child products. Column C shows the number of hot ^{2}D for that row. For each row, a Table similar to Table 12 is created, and the reaction rate is calculated. The resulting reaction rate is shown in Column D. At the bottom of Column D is the sum of all the reaction rates, 1.79×10^{12}. This is 6.43% of all energized ^{2}D.

The preliminary $^2D + ^2D$ reactions, at the very start of this example calculation, was 1.71×10^{12} reactions per second. This value, highlighted in green in Table 13, is the number of subsequent $^2D + ^2D$ reactions that occur, as a direct result of the energy released from those preliminary $^2D + ^2D$ reaction.

Recall that in the expanded loaded core, with 95% loading of ^2D, the density of the deuterium fuel is 5.387×10^{22}. The size of the palladium reactor core, 2 cm^3 prior to loading, is similar in volume to an LENR reactor typically used in experiments. The initial reaction rate was assumed to be 1.71×10^{12}, which is the value needed to get 1 watt of power from the two primary reactions. In order for a chain reaction to occur, this reactor must get at least that same number, 1.71×10^{12}, of subsequent reactions per second of $^2D+^2D$. As can be seen in the number highlighted in green in Table 13, this example reactor is able to get slightly more than that, with 1.79×10^{12} reactions $^2D+^2D$ per second. This means that a chain reaction is able to occur, and that the reaction rate would continue to increase until a steady state condition is reached.

Thus, this extensive calculation has shown that a chain reaction can indeed occur in an LENR palladium-deuteride electrolytic reactor.

6. Experimental Evidence in Agreement with this Model

It is well known experimentally that this reaction of $^2D+^2D \rightarrow {}^3He+n$ or the ^3H+p are that reactions that occur when a deuterated lattice contains energetic charged ionic particles. These are the reactions that occur as a result of a deuterated lattice having energetic ion particles traversing through it, regardless of how those energy ionic particles are introduced into the lattice. There are numerous examples that can be cited to confirm this experimental result.

In 2016, researchers irradiated targets of deuterides TiD_2, ZrD_2, NbD, and CrD_2 in experiments on the study of D-to-D reactions at astrophysical energies [39].

In the deuterated metal lattices, they irradiated the samples with low-energy deuterons, and they found not only the expected reaction of $^2D+^2D \rightarrow {}^3He+n$, but also that this reaction was dependent on the crystal orientation, due to the channeling effect. They also found effects that were attributed to electron screening.

> "It was experimentally observed for the first time that the neutron yield from the D(d, n)^{3}He reaction in titanium deuteride (TiD_2) with the [100] texture at ultralow deuteron collision energies is enhanced as compared with the reaction in a target with the [111] texture. .... On the basis of the experimental results, it was assumed that the observed increase in the yield from the D(d, n)^{3}He reaction was due to the deuteron channeling in the target crystal structure. The investigation of the dd reaction mechanisms in titanium deuteride targets and the analysis of the data with allowance for the crystalline state of the target cannot disprove the popular model of electron screening of interacting deuterons in a deuterium-saturated metal target."

It should be noted that these reactions occur at low energies, not just the high energies of a plasma. As is claimed in this model, these primary and secondary reactions are indeed the reactions that occur, and they occur regardless of the projectile ion energy. Experimentalists do not see an enhancement of the ^2D to ^2D ^4He reaction. Even if the ions are at low energies, the exact same reactions—the primary and secondary reactions that I have listed in this model—are the ones that take place, there is no change or dependence of that on projectile energy.

In another recent paper the observed reactions and by-products confirm this model of primary and secondary reactions [8], [40]. By bombarding deuterated metals with neutrons, the researchers found that the neutrons were able to transfer they kinetic energy to the fuel deuterons, which in turn caused a $^2D+^2D$ reaction. The resulting reactions and by-products were those described in this paper. They also saw effects of electron screening and changes in the effective astrophysical factor S(E). They evaluated the effects of screening on Coulomb scattering, localized heating of the cold fuel, and primary and subsequent reactions within the lattice. "The effect of screening for the enhancement of the total nuclear reaction rate is a function of multiple parameters including fuel temperature and the relative scattering probability between the fuel and the lattice metal nuclei."

The researchers found that electron screening is essential for efficient nuclear fusion reactions to occur. Screening effects in deuterated metals were demonstrated to be important on fusion reactions rates due to two primary factors–the Coulomb scattering of the projectile nuclei on the target nuclei, and the tunneling of the Coulomb barrier. During elastic scattering of charged particles on cold deuterons, some of the projectile's kinetic energy is transferred to the target deuteron. If enough kinetic energy is transferred to the deuteron, to overcome the Coulomb barrier, a subsequent nuclear fusion reaction is enabled. When the energetic deuterons interact with the lattice in a highly screened environment, electron screening plays a significant role in this transference process of kinetic energy. The researchers also noted, as described in this paper, that energetic neutrons have a superior efficiency of transferring kinetic energy to target deuterons, resulting in subsequent reactions. They determined that such a process, involving the neutrons, is a key ingredient in achieving and sustaining nuclear reactions. By bombarding the deuterated materials with neutrons, they saw evidence of energy transference from the neutrons to the deuterium fuel, and they saw evidence of subsequent ^{2}D+^{2}D ^{3}He+n reactions, specifically the energetic child product neutrons.

Numerous experimenters have performed studies wherein deuterons were bombarded into deuterated metals. These studies have measured substantially increased reaction rates over gaseous deuterium targets, implying that the electron clouds in the metal targets do indeed screen the positive ion charge, thus reducing the Coulomb barrier and leading to higher a cross section [41], [42], [43], [44], [45].

In reference [8], the researchers claim, based on analysis results, that neutrons are used to effectively heat deuterons. When the hot neutrons scatter, they efficiently deliver nearly one-half of their energy to a cold fuel deuteron, thereby turning it into an energetic deuteron. This newly-formed energetic deuteron is then able to interact with another nearby cold deuteron, in this highly electron-screened environment, leading to efficient nuclear tunneling and a subsequent fusion (D + $d \rightarrow n$ + 3He) reaction. Such a process, as described by these researchers, is exactly the process outlined in this model.

7. Conclusions

All of the so-called "miracles" of LENR are explained. The Coulomb barrier is overcome by the transference of kinetic energy to the cold ^{2}D via collisions of the cold ^{2}D with the energetic child products of the previous reactions. Neutrons are indeed emitted from the reactions; however, very few, if any escape the apparatus. (This is discussed and shown mathematically in the companion paper to this, "A Semi-Conventional Explanation for LENR, Part 2". It is also shown in this companion paper that only a small amount of gamma radiation occurs.)

The energy total produced by the reactor core, including the primary and secondary reactions is 3.384 watts (2.112 $\times$ 10^{13} MeV), and the number of ^{4}He atoms is 8.377 $\times$ 10^{11}. Thus, the ratio of energy per ^{4}He is 25.21 MeV per ^{4}He. Experimentally, this number many vary depending on how the experimental measurements actually measure the heat and the ^{4}He that are emitted from the tertiary reactions outside of the palladium core.

The size, shape, and deuteron density of the palladium core are parameters that can affect the overall reaction rates, but this is true more so for neutron scattering and neutron reactions than it is for charged-particle interactions. A second important consideration on the reaction rates is the mitigation of the electronic stopping phenomenon within the lattice of the PdD_x. As mentioned previously throughout this paper, this consideration of mitigated electronic stopping has been assumed for the calculations within this paper. Due to the unusual and diverse behavior of the PdD_x metal-hydride, its electronic stopping behavior as a function of loading $\times$ is an interesting and provocative topic for future experimental and theoretical research.

A better understanding of the material science of the PdD_x lattice–and how it affects the reaction and scattering rates of nuclides–is required to better understand this phenomenon. Aside from the presumed lattice-assistance, no highly unusual or novel physics is involved in these calculations; these calculations simply apply conventional nuclear engineering and conventional nuclear physics calculations to LENR.

A self-sustaining chain reaction is able to occur in an LENR palladium-deuteride electrolytic reactor, as seen by the rigorously calculated mathematical example of this paper, using typical parameters and reasonable estimates. High ^{2}D concentrations is required. Lattice assistance to mitigate the effects of electron stopping is required. This paper, and the calculations herein, show that Low Energy Nuclear Reactions are theoretically possible.

References

[1] Fleischmann, Martin; Pons, Stanley (1989), "Electrochemically induced nuclear fusion of deuterium", Journal of Electroanalytical Chemistry, 261 (2A): 301–308, doi:10.1016/0022-0728(89)80006-3 (first experiment.)

[2] Edmund Storms, The Science of Low Energy Nuclear Reactions, World Scientific Publishing Co. Pte. Ltd. 27 Warren Street, Suite 401, Hackensack, NJ 07601, pp. 53–61. (2007). ISBN-13 978-981-270-620-1 (hundreds of other experiments.)

[3] P. L. Hagelstein, "A unified model for anomalies in metal deuterides," Proceedings of the 8th International Conference on Cold Fusion, May 2000 Lerici (La Spezia), Italy. Edited by F. Scaramuzzi, p. 363.

[4] P.L. Hagelstein, I.U. Chaudhary, Phonon models for anomalies in condensed matter nuclear science, Current Science 108 (2015) 507–13.

[5] V.I. Vysotskii, M.V. Vysotskyy. Coherent correlated states and low-energy nuclear reactions in non stationary systems. European Phys. Journal. A (2013) v.49 issue 8:99 (2013), p. 1–12;

[6] Swartz, M. R, Active LANR Systems Emit a 327.37 MHz Maser Line, Proc. ICCF-22, J. Condensed Matter Nucl. Sci., Volume 33, pages 80–110 (2020)

[7] A. Takahashi, Physics of Cold Fusion by TSC Theory, J. Condensed Matter Nucl. Sci. 12 (2013) 1–14.

[8] Pines, Vladimir, et al.: Nuclear Fusion Reactions in Deuterated Metals. Phys. Rev. C (NASA/TP—2020- 5001617), vol. 101, 2020, p. 044609.

[9] K. Czerski, Enhanced electron screening and nuclear mechanism of cold fusion, in: V. Violante, F. Sarto (Eds), 15th International Conference on Condensed Matter Nuclear Science, ENEA, Italy, Rome, Italy, 2009, pp. 197–202.

[10] Edmund Storms, The Science of Low Energy Nuclear Reactions, World Scientific Publishing Co. Pte. Ltd. 27 Warren Street, Suite 401, Hackensack, NJ 07601, pp. 173–186. (2007). ISBN-13 978-981-270-620-1.

[11] Jean-Paul Biberian, Cold Fusion, Advances in Condensed Matter Nuclear Science, Elsevier, Amsterdam, (2020). pp. 265–367. ISBN-13: 978-0128159446.

[12] Jean-Paul Biberian, Fusion in All Its Forms, Infinite Energy Press, Concord, NH, (2015) pp. 91–96. ISBN 978-1-892925-11-4.

[13] National Nuclear Data Center, information extracted from the NuDat 2 database, http://www.nndc.bnl.gov/nudat2/

[14] Rutherford, E. (1911). "The Scattering of α and β rays by Matter and the Structure of the Atom". *Philosophical Magazine*. **6**: 21.

[15] "Scanning electron microscopy (SEM) and transmission electron microscopy (TEM) for materials characterization," B.J. Inkson, "Materials Characterization Using Nondestructive Evaluation (NDE) Methods," 2016. https://www.sciencedirect.com/topics/chemistry/elastic-scattering

[16] Podgoršak, E.B. (2016). Coulomb Scattering. In: Radiation Physics for Medical Physicists. Graduate Texts in Physics. Springer, Cham. https://doi.org/10.1007/978-3-319-25382-4_2

[17] S.S. Setayandeh, C.J. Webb, E. MacA. Gray. Electron and phonon band structures of palladium and palladium hydride: A review. Progress in Solid State Chemistry. Volume 60, 100285, (2020). https://doi.org/10.1016/j.progsolidstchem.2020.100285.

[18] F.D. Manchester, A. San-Martin, and J.M. Pitre. The H-Pd (hydrogen-palladium) system, Journal of Phase Equilibrial. Vol. 15 (1994) 62–83.

[19] Robinson, Mark T.; Oen, O. S. (1963). "The Channeling of Energetic Atoms in Crystal Lattices". Applied Physics Letters. 2(2): 30. Bibcode: 1963ApPhL...2...30R. doi:10.1063/1.1753757.

[20] Gemmell, D. S. (1974). "Channeling and related effects in the motion of charged particles through crystals". Rev. Mod. Phys. 46 (1):129. Bibcode:1974RvMP...46..129G. doi:10.1103/RevModPhys.46.129.

[21] Robinson, Mark T.; Oen, Ordean S. (1963-12-15). "Computer Studies of the Slowing Down of Energetic Atoms in Crystals". Physical Review. 132 (6): 2385–2398. doi: 10.1103/PhysRev.132.2385.

[22] https://en.wikipedia.org/wiki/Stopping_power_(particle_radiation)#:∼:text=Channeling,-Main%20article%3A%20Channelling&text=In%20crystalline%20materials%20the%20ion,be%20weaker%20in%20the%20channel.
[23] https://en.wikipedia.org/wiki/Channelling_(physics)]
[24] Akito Takahashi. A Theoretical Summary of Condensed Matter Nuclear Effects. J. Condensed Matter Nucl. Sci. 1 (2007) 1–13.
[25] Alfredo A Correa, "Calculating electronic stopping power in materials from first principles", Lawrence Livermore National Laboratory, LLNL-JRNL-749257. (2018).
[26] J. Kasagi, H. Yuki, T. Baba and T. Noda, "Low Energy Nuclear Fusion Reactions in Solids", 8th International Conference on Cold Fusion. Italy: Italian Physical Society, Bologna, Italy. Lerici (La Spezia), (2000) Figure 4.
[27] H C Jamieson and F D Manchester, "The magnetic susceptibility of Pd, PdH and PdD between 4 and 300 K", 1972 *J. Phys. F: Met. Phys.* 2 323 DOI 10.1088/0305-4608/2/2/023
[28] Kawae, Tatsuya; Inagaki, Yuji; Wen, Si; Hirota, Souhei; Itou, Daiki; Kimura, Takashi. Superconductivity in Palladium Hydride Systems. Journal of the Physical Society of Japan. 89 (5): 051004. (15 May 2020) doi:10.7566/JPSJ.89.051004.
[29] Ginsberg, Donald M. "superconductivity". *Encyclopedia Britannica*, 20 Sep. 2024, https://www.britannica.com/science/superconductivity. Accessed 4 November 2024.
[30] N. Ishikawa et al, Electronic excitation effects in ion-irradiated high-Tc superconductors, Nuclear Instruments and Methods in Physics Research B 135 (1998) 184–189.
[31] J.C. Barbour, E.L. Venturini, D.S. Ginley, J.F. Kwak. Irradiation effects in high temperature superconductors. Nuclear Instruments and Methods in Physics Research Section B: Beam Interactions with Materials and Atoms, Volume 65, Issues 1–4, 1 March 1992, Pages IN9, 531–538. https://doi.org/10.1016/0168-583X(92)95100-6
[32] N. Ishikawa, A. Iwase, Y. Chimi, H. Maeta, K. Tsuru, O. Michikami. Lattice expansion in EuBa2Cu3Oyirradiated with energetic ions. Physica C: Superconductivity and its Applications Volume 259, Issues 1–2, 1 March 1996, Pages 54-60. https://doi.org/10.1016/0921-4534(96)00022-6
[33] N Ishikawa, Y Chimi, A Iwase, K Tsuru, O Michikami. Defect production and recovery in high-Tc superconductors irradiated with electrons and ions at low temperature. Journal of Nuclear Materials Volumes 258–263, Part 2, October 1998, Pages 1924-1928. https://www.sciencedirect.com/science/article/abs/pii/S0022311598002244
[34] N. Ishikawa, Y. Chimi, A. Iwase, H. Maeta, K. Tsuru, O. Michikami, T. Kambara T. Mitamura, Y. Awaya, M. Terasawa. Electronic excitation effects in ion-irradiated high-Tc superconductors. Nuclear Instruments and Methods in Physics Research B 135 (1998) 184±189. http://www2.riken.jp/ap/publication/files/IshikawaN_NIMB135.pdf
[35] J. Lilley, Nuclear Physics, Principles and Applications, John Wiley and Sons, Ltd, New York, (2001). ISBN-0 471 97936 8. p. 147.
[36] Janus database, neutron scattering off 2D. https://www.oecd-nea.org/janisweb/book/neutrons/H2/MT2/renderer/811
[37] Janus database, neutron scattering of Pd https://www.oecd-nea.org/janisweb/book/neutrons/Pd105/MT2/renderer/811
[38] Lawson, J. D. (December 1955). Some criteria for a useful thermonuclear reactor (PDF) (Technical report). Atomic Energy Research Establishment, Harwell, Berkshire, U. K.
[39] V.M. Bystritsky, G.N. Dudkin, M. Filipowicz, Yu.Zh. Tuleushev, E.A. Zhakanbaev. Targets of deuterides TiD2, ZrD2, NbD, and CrD2 with different structures used in experiments on the study of pd and dd reactions at astrophysical energies. Nuclear Instruments and Methods in Physics Research Section A: Accelerators, Spectrometers, Detectors and Associated Equipment. Volume 810, 21 February 2016, Pages 80–85. https://doi.org/10.1016/j.nima.2015.12.006
[40] Steinetz, B.M., et al.: Novel Nuclear Reactions Observed in Bremsstrahlung-Irradiated Deuterated Metals (NASA/TP—2020-5001616), Phys. Rev. C, vol. 101, no. 4, 2020, p. 044640. https://journals.aps.org/prc/abstract/10.1103/PhysRevC.101.044610 Accessed May 21, 2020.
[41] Huke, A., et al.: Enhancement of Deuteron-Fusion Reactions in Metals and Experimental Implications. Phys. Rev. C, vol. 78, 2008, p. 015803. https://journals.aps.org/prc/abstract/ 10.1103/PhysRevC.78.015803.
[42] Czerski, K.: Enhancement of the Electron Screening Effect for d + d Fusion Reactions in Metallic Environments. Europhys. Lett., vol. 54, no. 4, 2001, p. 449. https://iopscience.iop.org/ article/10.1209/epl/i2001-00265-7.

[43] Raiola, F., et al.: Eur. Phys. J. A, vol. 13, 2002, pp. 377–382. Enhanced electron screening in d (d, p)t for deuterated Ta.https://link.springer.com/article/10.1007%2Fs10050-002-8766-5 Accessed May 20, 2022.

[44] Raiola, F., et al.: Electron Screening in d(d, p)t for Deuterated Metals and the Periodic Table. Phys. Lett. B, vol. 547, 2002, pp. 193–199. https://link.springer.com/article/ 10.1007%2Fs10050-002-8766-5 Accessed May 20, 2020.

[45] Bystritskii, V.M., et al.: Effect of *pd* and *dd* Reactions Enhancement in Deuterides TiD2, ZrD2 and Ta2D in the Astrophysical Energy Range. Phys. Part. Nucl. Lett., vol. 13, 2016, pp. 79–97. https://tpu.pure.elsevier.com/en/